Applied Intelligence (2026) 56:48
https://doi.org/10.1007/s10489-026-07085-5

Event-triggered fixed-time adaptive control for constrained nonlinear systems with input dead-zone and saturation

Mohamed Kharrat[1] · **Paolo Mercorelli**[2]

Received: 23 September 2025 / Accepted: 31 December 2025

Abstract

This paper addresses the issue of fixed-time neural adaptive event-triggered control for nonstrict-feedback nonlinear systems with full-state constraints, input dead-zone, and saturation. Radial basis function neural networks (RBFNNs) are used to identify the unknown nonlinearities. The paper considers both input saturation and dead-zone effects, approximating these non-smooth nonlinearities with a non-affine smooth function and then transforming them into an affine form using the mean value theorem. The approach integrates backstepping recursive design with a varying threshold event-triggered condition to create an event-triggered neural adaptive fixed-time control algorithm that employs barrier Lyapunov functions (BLFs) and RBFNNs. By applying the fixed-time stability criterion, the proposed controller ensures that the tracking error converges to a smaller region within a fixed time and that all variables in the closed-loop system remain bounded. Finally, two simulation examples are provided to demonstrate the effectiveness of the proposed method.

Keywords Nonlinear system · Event-triggered · Fixed-time stability · Dead-zone and saturation · Pendulum system

1 Introduction

Over the past decades, the control of nonlinear systems has emerged as a significant area of research, leading to the development of numerous methodologies for controller design. Among these, the adaptive backstepping technique stands out as a powerful advancement in nonlinear control [1–4]. This method offers a structured approach to synthesis by selecting appropriate Lyapunov functions at each step of the recursive design process, effectively addressing a class of nonlinear systems with either known functions or unknown constant coefficients. Early research often assumed that system nonlinearities were known a priori or could be linearly parameterized, which is impractical for many real-world systems. However, the excellent approximation capabilities of fuzzy logic systems (FLSs) and neural networks (NNs) have made it possible to approximate unknown nonlinear functions with arbitrary precision, thereby overcoming this limitation. Intelligent approaches such as fuzzy Bayesian belief networks and neural network–based controllers have been widely used to handle uncertainties and strong nonlinearities in engineering systems. These methods enable effective risk assessment in engineering, procurement, and construction pipeline projects, accurate trajectory tracking in humanoid robots, and improved power tracking and voltage regulation in nonlinear grid-connected photovoltaic systems [5–7]. Significant progress has been made in the intelligent control of nonlinear systems [8–10]. For example, an adaptive fuzzy control method has been developed for nonlinear systems with predefined time and accuracy requirements [11]. This method uses fuzzy logic to achieve the desired control accuracy. In the context of nonstrict-feedback stochastic nonlinear systems, a fuzzy adaptive control method has been proposed to address stochastic uncertainties, ensuring effective control performance [12]. Additionally, an adaptive fuzzy control scheme has been introduced for stochastic high-order nonlinear systems, leveraging fuzzy logic to manage complex nonlinear dynamics [13]. For nonstrict-feedback nonlinear systems with input delay, an adaptive neural control method has been developed [14]. This approach utilizes neural networks to address input delay challenges, providing effective control for nonlinear systems with nonstrict-feedback structures.

✉ Paolo Mercorelli
paolo.mercorelli@leuphana.de

[1] Mathematics Department, College of Science, Jouf University, Sakaka, Saudi Arabia

[2] Institute for Production Technology and Systems, Leuphana University, Lueneburg 21335, Germany

Published online: 16 January 2026

It is important to note that the previously mentioned methods are not suitable for systems with constraints. In real-world applications, managing state constraints is crucial, and avoiding constraint violations holds significant practical value. Many researchers have focused on addressing state constraint issues [15–17]. For nonlinear multi-agent systems with full-state constraints and unmeasurable states, a neural adaptive control approach has been introduced [18]. This method employs neural networks to handle full-state constraints and optimize control performance even when states cannot be directly measured. Additionally, an adaptive neural network asymptotic tracking control technique has been developed for stochastic nonlinear systems with unknown control gains and full-state constraints [19]. This approach tackles uncertainties in control gains and ensures robust tracking performance. To manage state constraints in strict-feedback nonlinear systems, an observer-based neuro-adaptive optimized control strategy has been proposed [20]. This strategy uses neural networks and observers to optimize control under strict-feedback conditions. Furthermore, an adaptive neural asymptotic tracking method has been formulated for uncertain non-strict feedback systems with full-state constraints [21]. This method employs a command-filtered technique to achieve precise and robust tracking despite the presence of uncertainties. A composite neural learning–based adaptive control scheme has been proposed for autonomous surface vehicles with full-state constraints, where neural approximators compensate unknown nonlinear dynamics and actuator failures [22].

However, the aforementioned studies did not address nonstrict-feedback nonlinear systems with input saturation and dead zones, which can limit their practical engineering applications [23–26]. This study explicitly considers input saturation and dead zones, as these are significant sources of non-smooth nonlinearities in actuators that can severely impact control system performance and Recent research has focused on addressing these issues [27, 28]. For instance, an event-based adaptive neural network controller design has been proposed for strict-feedback discrete-time nonlinear systems, effectively tackling input dead zones and saturation by dynamically adjusting the controller based on system states and constraints [29]. Additionally, an output-feedback adaptive neural network control strategy has been developed for uncertain nonsmooth nonlinear systems, integrating neural networks to manage uncertainties and nonlinearities while accommodating input constraints [30]. Furthermore, adaptive fuzzy funnel control techniques have been introduced to handle nonlinear systems with input dead zones and saturation, utilizing fuzzy logic to manage complex nonlinearities and constraints and thereby improving control performance [31].

Although the existing literature has addressed control accuracy for various systems, the control efficiency remains relatively low. Rapid system response is essential, and to achieve this, finite-time control is often employed [32–34]. Finite-time control offers several benefits, including strong resistance to disturbances, short convergence times, high accuracy, and quick convergence. Consequently, finite-time control for nonlinear systems has garnered significant interest from researchers and has yielded impressive results [35–37]. However, finite-time control can be ineffective when the initial state is unknown, leading to suboptimal tracking performance. To address this limitation, the concept of fixed-time stability has been introduced [38]. Fixed-time control ensures that the system meets its control objectives within a predetermined time frame, even in the presence of constraints and disturbances [39, 40]. For nonlinear constrained multi-agent systems under the presence of input saturation an adaptive fixed-time control via fuzzy approximation has been reported, which ensures control objectives are achieved within fixed-time [41]. For strict-feedback nonlinear systems under the presence of input delays, fixed-time fuzzy adaptive fault-tolerant control maintains system performance and stability despite the presence of delays and faults [42]. Furthermore, dynamic event-based adaptive fixed-time control for uncertain strict-feedback nonlinear systems with state constraints adapts to changes and constraints, guaranteeing robust control within a fixed time [43]. A practical fixed-time adaptive control strategy has been presented for uncertain nonlinear systems with dead-zone constraints, ensuring fixed-time convergence of tracking errors while maintaining the boundedness of all closed-loop signals in the presence of input nonlinearities and system uncertainties [44].

Recently, networked control systems have seen rapid development due to their low cost, flexibility, reliability, and ease of installation. However, limited network bandwidth introduces challenges such as transmission delays and packet disorder [45–48]. To address these issues, an event-triggered control (ETC) approach has been proposed, which efficiently manages network resources. Building on ETC, several significant advancements have been made [49–53]. For nonlinear systems with constraints, a finite-time adaptive control offers a robust solution using command filters and event triggered mechanism [54]. This approach adapts to system changes and ensures adherence to constraints within a finite time frame. For stochastic nonlinear systems with unmeasured states, event-triggered finite-time adaptive fuzzy control addresses uncertainties and enhances control performance, even when certain states are not directly observable [55]. In the case of nonlinear systems, fuzzy adaptive finite-time tracking control using an event-triggered quantized control scheme ensures accurate

tracking and adaptation [56]. This method improves performance by reducing the effects of quantization and event-triggering. For nonlinear systems facing actuator failures, fixed-time adaptive event-triggered fault-tolerant control maintains system stability and performance within a fixed time period [57]. This approach effectively manages actuator faults and preserves control effectiveness. An adaptive global prescribed performance control approach has been developed for nonlinear Markov jumping systems with input saturation, where a threshold-based strategy ensures desired transient and steady-state performance. The effectiveness of the method is demonstrated through its application to a chemical reactor model under randomly switching dynamics [58].

Designing controllers for nonlinear systems in the presence of multiple constraints, such as full-state constraints, input saturation, and dead-zone nonlinearities, presents significant challenges. These constraints often occur simultaneously in practical engineering applications, for example in robotic manipulators used in industrial automation, unmanned aerial vehicles, or power-electronic systems. Actuator dead-zones appear due to mechanical play or nonlinear friction, input saturation arises from voltage or torque limits, and full-state constraints ensure that system states, such as joint angles, velocities, or currents, remain within safe operational bounds. These factors make the control design process more complex and achieving effective and reliable performance difficult. The practical importance of addressing these challenges motivates the development of advanced control strategies. Conventional finite-time control methods may fail when the initial states are unknown, leading to suboptimal tracking and possible violation of constraints. To overcome these challenges, adaptive fixed-time control schemes combined with event-triggered mechanisms inspire a promising solution. These approaches ensure robust tracking and system stability within a predetermined time while handling multiple constraints simultaneously, thereby improving both safety and performance in real-world scenarios.

The main contributions of this paper are as follows

(i) This paper introduces an adaptive neural fixed-time control approach for nonstrict-feedback nonlinear systems that simultaneously addresses full-state constraints, input dead-zone, and input saturation. Unlike finite-time control methods [35–37], where the convergence time depends on the initial state, the fixed-time property ensures that all system states reach the desired trajectory within a predetermined time regardless of initial conditions. The proposed method combines backstepping recursive design with a varying-threshold event-triggered mechanism, utilizing barrier Lyapunov functions and radial basis function neural networks to guarantee constraint satisfaction, reduce communication events, and avoid Zeno behavior.

(ii) Input saturation and dead-zone nonlinearities are incorporated directly into the controller design, overcoming limitations of previous studies [23–25] that often treat these effects separately. By approximating the non-smooth input nonlinearities with smooth non-affine functions and applying the mean value theorem, the system is transformed into an affine form suitable for backstepping design. This ensures robust handling of practical actuator limitations encountered in engineering systems.

(iii) The proposed control scheme ensures boundedness of all closed-loop signals and guarantees that the tracking error converges to a small neighborhood of the origin within a fixed-time. The integration of fixed-time stability, event-triggered control, and adaptive neural approximation provides a unified framework that improves tracking performance, enhances robustness against disturbances and uncertainties, and efficiently manages communication resources, highlighting the fundamental distinction and advantage over existing finite-time approaches.

The remaining sections of this paper are organized as follows: The problem formulation and some preliminary information are presented in the next section. The fixed-time adaptive control scheme's design and a thorough stability analysis are then given. The suggested controller is then validated through two simulation examples. Lastly, the last section summarizes the work's primary conclusions.

Notations The following notations are utilized in this paper: To denote the set of real numbers, use $\mathbb{R}$; The n -dimensional real space is represented by $\mathbb{R}^n$; the system output is denoted by y, the system input by u, and the actual control lae by v; The system state vector is represented by $\bar{\zeta}_i = [\zeta_1, \zeta_2, \ldots, \zeta_i]^T \in \mathbb{R}^i$ for $i = 1, 2, \ldots, n$; the Euclidean norm of a vector X is represented as $\|X\|$.

2 Problem formulation and preliminaries

Consider the nonlinear system in nonstrict-feedback form as

$$\begin{cases} \dot{\zeta}_i &= g_i(\bar{\zeta}_i)\zeta_{i+1} + f_i(\zeta), \quad 1 \le i \le n-1 \\ \dot{\zeta}_n &= g_n(\zeta_n)u + f_n(\zeta) \\ y &= \zeta_1 \end{cases} \tag{1}$$

where $\bar{\zeta}_i = [\zeta_1, \zeta_2, \ldots, \zeta_i]^T \in \mathbb{R}^i$ for $i = 1, 2, \ldots, n$ and $\zeta = [\zeta_1, \zeta_2, \ldots, \zeta_n]^T \in \mathbb{R}^i$ represent the system state

vector, $u \in \mathbb{R}$, and $y \in \mathbb{R}$ are the system input and system output, respectively. $f_i(\cdot) : \mathbb{R}^i \to \mathbb{R}$ and $g_i(\cdot) : \mathbb{R}^i \to \mathbb{R}$ are the unknown smooth nonlinear functions. In this work, we consider full-state constraints expressed as $|\zeta_i(t)| < k_{c_i}, \quad i = 1, \ldots, n, \ \forall t \geq 0$, where $k_{c_i} > 0$ are constant bounds chosen based on the physical limits and safety requirements of the system.

The nonsymmetric dead-zone and input saturation of the system, $u(v) \in \mathbb{R}$, is given as follows [31]

$$u(v) = \begin{cases} C_P, & \text{if } v \geq b_{vn} \\ t_r(v), & \text{if } b_{vm} < v < b_{vn} \\ 0, & \text{if } b_{ln} \leq v \leq b_{vm} \\ t_l(v), & \text{if } b_{lm} < v < b_{ln} \\ C_N, & \text{otherwise} \end{cases} \tag{2}$$

with $t_r(b_{vm}) = t_l(b_{ln}) = 0$, $t_r(b_{vn}) = CP$, $t_l(b_{lm}) = C_N$; $b_{lm} < b_{ln} < 0$ and $0 < b_{vm} < b_{vn}$ are unknown input nonlinearity parameters.. $t_r(v)$ and $t_l(v)$ represents nonlinear smooth unknown functions. The dead-zone and saturation input is denoted by v; the unknown saturation values are $C_P > 0$ and $C_N < 0$.

Assume the controller is implemented on a digital platform. Let $\{t_k\}_{k=0}^{\infty}$, where $t_0 = 0$ and $k \in \mathbb{Z}^+$ (with $\mathbb{Z}^+$ denoting the set of positive integers), represent the sequence of event-triggering instants generated by an event generator. The sample error is defined as [51]

$$m(t) = \omega(t) - u(t), \quad t \in [t_k, t_{k+1}), \tag{3}$$

where $\omega(t)$ denotes the continuous control input (details to be explained later), and $u(t) = \omega(t_k)$ represents the sampled control at $t = t_k$. Each interval $[t_k, t_{k+1})$ is treated as a cycle, during which $e(t)$ varies randomly and is reset to 0 at each t_k.

Control objective The aim is to develop an adaptive event-triggered fixed-time control strategy that ensures the system output y accurately tracks the desired trajectory y_d, while guaranteeing that all closed-loop signals are SGPFS and that the states always remain within the prescribed full-state constraint regions. Furthermore, the proposed input-triggering strategy significantly reduces the computational load related to the communication process.

The following lemmas and assumptions are offered in the developments that follow to support this.

Assumption 1 ([51]) The functions $g_i(\zeta_i)$, $i = 1, 2, \ldots, n$ are known, and there exist positive constants $\bar{g}_i$ and $\underline{g}_i$ such that

$$0 < \underline{g}_i \leq |g_i| \leq \bar{g}_i. \tag{4}$$

Remark 1 Assumption 1, which requires the functions $g_i(\zeta_i)$ to be known and bounded, ensures that the system satisfies the controllability condition and that the control input can effectively influence the system dynamics. This assumption is commonly adopted in adaptive backstepping design to facilitate stability analysis and guarantee fixed-time convergence. For practical systems where $g_i(\cdot)$ may be partially unknown, the proposed method can be extended by employing robust or adaptive estimation techniques, such as neural network approximators or adaptive bounding functions, to estimate or compensate for the unknown portions of $g_i(\zeta_i)$.

Assumption 2 ([52]) The target signal $y_d(t)$ and its derivatives $y_d^{(j)}(t)$, $j = 1, \ldots, n$ satisfy $|y_d(t)| \leq A_0 < \bar{\kappa}_1$ and $|y_d^{(j)}(t)| \leq A_j$, where $A_0, \ldots, A_n$ are positive constants.

Assumption 3 ([31]) There exist unknown positive constants b_{l1}, b_{l2}, b_{r1}, and b_{r2}, such that

$$0 < b_{l1} < t_l(v) < b_{l2} < \infty \quad \forall v \in [b_{lm}, b_{ln}] \tag{5}$$

$$0 < b_{r1} < t_r(v) < b_{r2} < \infty \quad \forall v \in [b_{vm}, b_{vn}] \tag{6}$$

where $t_r'(v)$ and $t_l'(v)$ are, respectively, the derivatives of $t_r(v)$ and $t_l(v)$ with respect to v.

Remark 2 It is evident from (2) that for a given v, the dead-zone and saturation might not necessarily be differentiable. We may approximate the value using the smooth function outlined in [31].

$$\begin{aligned} h(v) = {} & \frac{C_P}{2} \tanh\left(v - \frac{b_{vm}}{l_2} - \tau_r\right) + \frac{C_P}{2} \tanh(b_{vm} + \tau_r l_2) \\ & - \frac{C_N}{2} \tanh\left(v - \frac{b_{ln}}{l_1} + \tau_l\right) - \frac{C_N}{2} \tanh(b_{ln} - \tau_l l_1) \end{aligned} \tag{7}$$

where τ_r, τ_l, l_1, and l_2 are suitable positive parameters. The approximation errors can be minimized by appropriately selecting the positive parameters τ_r, τ_l, l_1, and l_2. These parameters govern the smoothness and accuracy of the function $h(v)$ used to approximate the dead-zone and saturation. Specifically, increasing τ_r and τ_l smooths the transitions near the dead-zone boundaries, while l_1 and l_2 influence the slopes at the saturation limits. In practical applications, these parameters should be chosen to ensure that the approximation error remains sufficiently small to maintain closed-loop stability. Small variations in these parameters have negligible impact on stability but may slightly affect tracking performance.

We are able to write (2) as

$$u(v) = h(v) + p(v) \tag{8}$$

where the approximation error is defined as $p(v) = u(v) - h(v)$, and from the definition of the dead-zone and saturation nonlinearity it follows that $|u(v)| \leq \max\{|C_P|, |C_N|\}$ for all admissible v. Moreover, since the hyperbolic tangent functions are bounded and under Assumption 2 the derivative $h'(v_u)$ is bounded for $v \in [-M_1, M_2]$, the smooth approximation $h(v)$ is also bounded on this compact set. Therefore, the approximation error satisfies

$$|p(v)| = |u(v) - h(v)| \leq |u(v)| + |h(v)| \leq P \tag{9}$$

where $P > 0$ is an unknown but finite constant. We know that there is a constant $\alpha \in (0, 1))$ obeying the mean-value theorem [31].

$$h(v) = h'(v_u)(v - v_0) + h(v_0) \tag{10}$$

where $v_u = \alpha v + (1 - \alpha)v_0$ and v_0 is a constant. When $v_0 = 0$, one has

$$h(v) = h'(v_u)v \tag{11}$$

$$\begin{aligned} h'(v_u) = {} & \frac{C_P l_2}{2}\left(\frac{1}{\cosh^2\left(l_2(v_u - \frac{b_{vm}}{l_2} - \tau_r)\right)}\right) \\ & - \frac{C_N l_1}{2}\left(\frac{1}{\cosh^2\left(l_1(v_u - \frac{b_{ln}}{l_1} + \tau_l)\right)}\right) \end{aligned} \tag{12}$$

Assumption 4 ([31]) For $v \in [-M_1, M_2]$ with $0 < M_1 < \infty$ and $0 < M_2 < \infty$, assume that

$$0 < m < h'(v_u) < \infty \tag{13}$$

where m is an unidentified positive constant.

Definition 1 ([51]) Consider a nonlinear system described by

$$\dot{\zeta} = f(\zeta, t), \quad \zeta(0) = \zeta_0 \tag{14}$$

where $f(\zeta, t)$ is an unknown smooth nonlinear function and $\zeta \in \mathbb{R}^n$ is the state variable. Assume that the Lyapunov function indicates that system (3) is stable. System (14) is fixed-time stable if, given any initial condition $\zeta(0) \in \Omega$, the system's solution can converge to a compact set Ω in a limited amount of time T_s, where T_s is bounded by $T_{\max}$.

Lemma 1 *([37]) As long as $|n| < 1$ and l is any positive integer, we have*

$$\log\left(\frac{1}{1 - n^{2l}}\right) < \frac{n^{2l}}{1 - n^{2l}} \tag{15}$$

holds.

Lemma 2 *([49]) For $\xi \in \mathbb{R}$ and $\epsilon > 0$ gives*

$$0 \leq |\xi| - \xi \tanh\left(\frac{\xi}{\epsilon}\right) \leq 0.2785\epsilon. \tag{16}$$

Lemma 3 *([52]) For constants $q > 1$ and $p \in (0, 1)$, we have*

$$\dot{V}(\zeta) \leq \varsigma V_n^q - \varrho V_n^p + \sigma, \quad \forall \zeta \in \mathbb{R}^n \tag{17}$$

where the system (14) is said to be practically fixed-time stable, and the settling time T_s is given by:

$$T_s = \frac{1}{\varsigma\pi(q-1)} + \frac{1}{\varrho\pi(1-p)} \tag{18}$$

where $\pi \in (0, 1)$. The residual set of the system (14) solution is as follows

$$\Omega = \left\{\zeta | V(\zeta) \leq \min\left\{\left(\frac{\sigma}{\varsigma(1-\pi)}\right)^{1/q}, \left(\frac{\sigma}{\varrho(1-\pi)}\right)^{1/p}\right\}\right\}. \tag{19}$$

Lemma 4 *([37]) For any given $(x, y) \in \mathbb{R}^2$; $a \in [1, \infty)$, $b \in [1, \infty)$, and $\epsilon \geq 0$ with $(a-1)(b-1) = 1$, the following relation holds:*

$$xy \leq \frac{e^{\epsilon}}{a}|x|^a + \frac{1}{b\epsilon^b}|y|^b \tag{20}$$

Lemma 5 *([51]) For any given positive constants b_1, b_2, b_3, and real variables x and y, we have:*

$$|x|^{b_1}|y|^{b_2} \leq \frac{b_1}{b_1 + b_2} b_3 |x|^{b_1 + b_2} + \frac{b_2}{b_1 + b_2} b_3^{-\frac{b_1}{b_2}} |y|^{b_1 + b_2}. \tag{21}$$

Lemma 6 *([37]) For $x_i \in \mathbb{R}$, $i = 1, \ldots, n$, the following inequalities hold:*

$$\left(\sum_{i=1}^{n} |x_i|\right)^k \leq \sum_{i=1}^{n} |x_i|^k \leq l^{k-1}\left(\sum_{i=1}^{n} |x_i|\right)^k, \tag{22}$$

where $0 < k \leq 1$.

Radial basis function neural networks (RBFNN) In this part, suppose that $f(Z) : \mathbb{R}^n \to \mathbb{R}$ is an unknown continuous

function over a compact set $\Omega_Z \subset \mathbb{R}^q$. At each step, it will be approximated by the RBFNNs$\hat{f}(Z) = W^{*T}S(Z)$. For any $\epsilon > 0$, the following equation holds [14]

$$\hat{f}(Z) = W^{*T}S(Z) + \delta(Z), \quad |\delta(Z)| \leq \epsilon, \tag{23}$$

where $W^* = [w_1^*, \ldots, w_N^*]^\top \in \mathbb{R}^N$ with $N > 1$ denotes the weight vector, and W^* is defined by

$$W^* = \arg \min_{W \in \mathbb{R}^l} \sup_{Z \in \Omega_Z} \left| f(Z) - W^{*T}S(Z) \right| \tag{24}$$

where $S(Z) = [s_1(Z), s_2(Z), \ldots, s_N(Z)]^\top$ is the basis function vector with $s_i(Z)$ given by the Gaussian function:

$$s_i(Z) = \exp\left[-\frac{(Z-\mu_i)^\top (Z-\mu_i)}{\eta^2} \right], \quad i = 1, 2, \ldots, N, \tag{25}$$

where $\mu_i = [\mu_{i1}, \mu_{i2}, \ldots, \mu_{iN}]^T$ and η represents the width of the Gaussian function.

Lemma 7 *[14] Consider a neural network whose radial basis function vector is defined as* $S(Z_n) = [s_1(Z_n), \ldots, s_N(Z_n)]^T$, *where the input vector is given by* $Z_n = [z_1, \ldots, z_n]^T$. *Then, for any* $m \leq n$, *one has* $\|S(Z_n)\|^2 \leq \|S(Z_m)\|^2$.

3 The controller design and stability analysis

This section will structure the stability analysis procedure and develop an adaptive event-triggered fixed-time controller for nonlinear systems. There are n steps in the backstepping recursive design technique. The common coordinate transformation is defined as follows to start:

$$\begin{aligned} z_1 &= \zeta_1 - y_d \\ z_i &= \zeta_i - \alpha_{i-1}, \quad i = 2, 3, \ldots, n \end{aligned} \tag{26}$$

where α_{i-1} represents the virtual controller, y_d is the reference output signal, and z_i denotes the tracking error.

Step 1: From (1) and (26), we have

$$\begin{aligned} \dot{z}_1 &= g_1\zeta_2 + f_1 - \dot{y}_d \\ &= g_1 (z_2 + \alpha_1) + f_1 - \dot{y}_d. \end{aligned} \tag{27}$$

The Barrier Lyapunov Function (BLF) is formulated as

$$V_1 = \frac{1}{2} \log\left(\frac{\kappa_1^2}{\kappa_1^2 - z_1^2} \right) + \frac{\underline{g}_1}{2\mu_1} \tilde{\theta}_1^2 \tag{28}$$

where $\kappa_1 > |z_1|$, $\mu_1 > 0$, and $\kappa_1 = \bar{\kappa}_1 - Y_0$; $\hat{\theta}_1$ is the estimation of θ_1, and $\tilde{\theta}_1 = \theta_1 - \hat{\theta}_1$.

Computing the derivative of V_1 gives

$$\dot{V}_1 = \bar{z}_1 \left(\varphi_1 (z_2 + \alpha_1) + \bar{f}_1(Z_1) \right) - \frac{1}{\mu_1} \varphi_1 \tilde{\theta}_1 \dot{\hat{\theta}}_1 \tag{29}$$

where $\bar{z}_1 = \frac{z_1}{\kappa_1^2 - z_1^2}$, $\bar{f}_1(Z_1) = f_1 - \dot{y}_d$, and $Z_1 = [\zeta, y_d, \dot{y}_d]^T$.

Since $\bar{f}_1(Z_1)$ contains the unknown smooth function f_1. Then, RBFNN $W_1^{*T}S_1(Z_1)$ is applied to model $\bar{f}_1(Z_1)$ such that for any constant $\epsilon_1 > 0$

$$\bar{f}_1(Z_1) = W_1^T S_1(Z_1) + \delta_1(Z_1), |\delta_1(Z_1)| \leq \epsilon_1. \tag{30}$$

By applying Lemma 7 and using the method of completing the square, one has

$$\begin{aligned} \bar{f}_1(Z_1) &= \bar{z}_1 \left(W_1^{*T} S_1(Z_1) + \delta_1(Z_1) \right) \\ &\leq |\bar{z}_1| \left(\|W_1^*\| \|S_1(Z_1)\| + \epsilon_1 \right) \\ &\leq |\bar{z}_1| \left(\|W_1^*\| \|S_1(Z_1)\| + \epsilon_1 \right) \\ &\leq \frac{1}{2a_1^2} \bar{z}_1^2 \theta_1 \underline{g}_1 S_1^T(X_1) S_1(X_1) + \frac{a_1^2}{2} + \frac{\bar{z}_1^2 \underline{g}_1}{2} + \frac{\epsilon_1^2}{2\underline{g}_1}, \end{aligned} \tag{31}$$

where $a_1 > 0$ is a design parameter, $\theta_1 = \|W_1^*\|^2 / \underline{g}_1$ and $X_1 = [\zeta_1, y_d, \dot{y}_d]^T$.

By using (31) into (29), one has

$$\begin{aligned} \dot{V}_1 \leq\ & \bar{z}_1 \left(\varphi_1 \alpha_1 + \frac{\bar{z}_1 \hat{\theta}_1 \underline{g}_1 S_1^T(X_1) S_1(X_1)}{2a_1^2} + \frac{\bar{z}_1 \underline{g}_1}{2} \right) \\ & - \frac{\underline{g}_1}{\mu_1} \tilde{\theta}_1 \left(\dot{\hat{\theta}}_1 - \frac{\bar{z}_1^2 S_1^T(X_1) S_1(X_1) \mu_1}{2a_1^2} \right) \\ & + \bar{z}_1 z_2 g_1 + \frac{a_1^2}{2} + \frac{\epsilon_1^2}{2\underline{g}_1}. \end{aligned} \tag{32}$$

Next, the virtual control signal α_1 and the adaptive law $\hat{\theta}_1$ are formulated as follows

$$\alpha_1 = -\frac{b_1 z_1^3}{\kappa_1^2 - z_1^2} - \frac{c_1 z^{2p-1}}{(\kappa_1^2 - z_1^2)^{p-1}} - \frac{\bar{z}_1 \hat{\theta}_1 S_1^T(X_1) S_1(X_1)}{2a_1^2} - \frac{\bar{z}_1^2}{2}, \tag{33}$$

$$\dot{\hat{\theta}}_1 = \frac{\bar{z}_1^2 S_1^T(X_1) S_1(X_1) \mu_1}{2a_1^2} - \eta_1 \hat{\theta}_1 - \frac{\varkappa_1}{\mu_1} \hat{\theta}_1^3 \tag{34}$$

where $b_1 > 0$, $p \in \left(\frac{1}{2}, 1\right)$, $c_1 > 0$, $\varkappa_1 > 0$, and $\eta_1 > 0$ represents the design parameters.

Substituting (33) and (34) into (32) gives

$$\dot{V}_1 \leq -\frac{b_1 \underline{g}_1 z_1^4}{(\kappa_1^2 - z_1^2)^2} - \frac{c_1 \underline{g}_1 z_1^{2p}}{(\kappa_1^2 - z_1^2)^p} + \frac{\eta_1 \underline{g}_1}{\mu_1} \tilde{\theta}_1 \hat{\theta}_1 + \frac{\varkappa_1 \underline{g}_1}{\mu_1^2} \tilde{\theta}_1 \hat{\theta}_1^3 + \bar{z}_1 z_2 g_1 + \frac{a_1^2}{2} + \frac{\epsilon_1^2}{2\underline{g}_1}. \tag{35}$$

Remark 3 The inequality (35) is valid if $\theta_1(t) \geq 0$. Therefore, to ensure $\theta_1(t) \geq 0$ for all $t \geq 0$, it is necessary that $\hat{\theta}_1(0) \geq 0$. Likewise, in the subsequent analysis, it is required that $\hat{\theta}_i(0) \geq 0$ for $i = 2, 3, \ldots, n$. Additionally, to prevent the singularity of $\frac{c_1 z_1^{2p-1}}{(\kappa_1^2 - z_1^2)^{p-1}}$, the parameter p is selected within the range $\left(\frac{1}{2}, 1\right)$.

Step i: From (1) and (9), we have

$$\begin{aligned} \dot{z}_i &= g_i \zeta_{i+1} + f_i - \dot{\alpha}_{i-1} \\ &= g_i \left(z_{i+1} + \alpha_i\right) + f_i - \dot{\alpha}_{i-1}. \end{aligned} \tag{36}$$

Design the BLF V_i as follows

$$V_i = V_{i-1} + \frac{1}{2} \log \frac{\kappa_i^2}{\kappa_i^2 - z_i^2} + \frac{\underline{g}_1}{2\mu_i} \tilde{\theta}_i^2 \tag{37}$$

where $\kappa_i > |z_i|$, $\mu_i > 0$, $\tilde{\theta}_i = \theta_i - \hat{\theta}_i$, and $\hat{\theta}_i$ is the estimation of θ_i. The time derivatives of V_i gives

$$\dot{V}_i = \dot{V}_{i-1} + \bar{z}_i \left(g_i \left(z_{i+1} + \alpha_i\right) + \bar{f}_i(Z_i)\right) - \frac{\underline{g}_1}{\mu_i} \tilde{\theta}_i \dot{\hat{\theta}}_i - \bar{z}_{i-1} g_{i-1} z_i \tag{38}$$

where $\bar{z}_i = \frac{z_i}{\kappa_i^2 - z_i^2}$,

$\bar{f}_i(Z_i) = f_i + \bar{z}_{i-1} g_{i-1} (\kappa_i^2 - z_i^2) - \dot{\alpha}_{i-1}$, and

$Z_i = \left[\zeta_1, \zeta_2, \ldots, \zeta_n, y_d, \dot{y}_d, \ldots, y_d^{(i-1)}, \hat{\theta}_1, \hat{\theta}_2, \ldots, \hat{\theta}_{i-1}, \hat{\theta}_1, \hat{\theta}_2, \ldots, \hat{\theta}_{i-1}\right]^T$.

Since $\bar{f}_i(Z_i)$ contains the unknown smooth function f_i, then RBFNN $W_i^{*T} S_i(Z_i)$ is applied to model $\bar{f}_i(Z_i)$ such that for any constant $\epsilon_i > 0$:

$$\bar{f}_i(Z_i) = W_i^T S_i(Z_i) + \delta_i(Z_i), \quad |\delta_i(Z_i)| \leq \epsilon_i. \tag{39}$$

By applying Lemma 7 and using the method of completing the square, one has

$$\begin{aligned} \bar{f}_i(Z_i) &= \bar{z}_i \left(W_i^{*T} S_i(Z_i) + \delta_i(Z_i)\right) \\ &\leq |\bar{z}_i| \left(\|W_i^*\| \|S_i(Z_i)\| + \epsilon_i\right) \\ &\leq |\bar{z}_i| \left(\|W_i^*\| \|S_i(Z_i)\| + \epsilon_i\right) \\ &\leq \frac{1}{2a_i^2} \bar{z}_i^2 \theta_i \underline{g}_i S_i^T(X_i) S_i(X_i) + \frac{a_i^2}{2} + \frac{\bar{z}_i^2 \underline{g}_i}{2} + \frac{\epsilon_i^2}{2\underline{g}_i}, \end{aligned} \tag{40}$$

where $Z_i = \left[\zeta_1, \zeta_2, \ldots, \zeta_i, y_d, \dot{y}_d, \ldots, y_d^{(i-1)}, \hat{\theta}_1, \hat{\theta}_2, \ldots, \hat{\theta}_{i-1}, \hat{\theta}_1, \hat{\theta}_2, \ldots, \hat{\theta}_{i-1}\right]^T$, $a_i > 0$ is a design parameter, and $\theta_i = \|W_i^*\|^2 / \underline{g}_i$

By using (40) into (38), we have

$$\begin{aligned} \dot{V}_i \leq \dot{V}_{i-1} &+ \bar{z}_i \left(g_i \alpha_i + \frac{\bar{z}_i \hat{\theta}_i \underline{g}_i S_i^T(X_i) S_i(X_i)}{2a_i^2} + \frac{\bar{z}_i \underline{g}_i}{2}\right) \\ &- \frac{\underline{g}_i}{\mu_i} \tilde{\theta}_i \left(\dot{\hat{\theta}}_i - \frac{\bar{z}_i^2 S_i^T(X_i) S_i(X_i) \mu_i}{2a_i^2}\right) + \bar{z}_i z_{i+1} g_i - \bar{z}_{i-1} z_i g_{i-1} + \frac{a_i^2}{2} + \frac{\epsilon_i^2}{2\underline{g}_i}. \end{aligned} \tag{41}$$

Next, the virtual control signal α_i and the adaptive law $\hat{\theta}_i$ are formulated as follows:

$$\alpha_i = -\frac{b_i z_i^3}{\kappa_i^2 - z_i^2} - \frac{c_i z^{2p-1}}{(\kappa_i^2 - z_i^2)^{p-1}} - \frac{\bar{z}_i \hat{\theta}_i S_i^T(X_i) S_i(X_i)}{2a_i^2} - \frac{\bar{z}_i^2}{2}, \tag{42}$$

$$\dot{\hat{\theta}}_i = \frac{\bar{z}_i^2 S_i^T(X_i) S_i(X_i) \mu_i}{2a_i^2} - \eta_i \hat{\theta}_i - \frac{\zeta_i}{\mu_i} \hat{\theta}_i^3 \tag{43}$$

where $b_i > 0$, $p \in \left(\frac{1}{2}, 1\right)$, $c_i > 0$, $\varkappa_i > 0$, and $\eta_i > 0$ represent the design parameters.

By using (42) and (43) into (41), one has

$$\begin{aligned} \dot{V}_i \leq \dot{V}_{i-1} &- \frac{b_i \underline{g}_i z_i^4}{(\kappa_i^2 - z_i^2)^2} - \frac{c_i \underline{g}_i z_i^{2p}}{(\kappa_i^2 - z_i^2)^p} + \frac{\eta_i \underline{g}_i}{\mu_i} \tilde{\theta}_i \hat{\theta}_i + \frac{\varkappa_i \underline{g}_i}{\mu_i^2} \tilde{\theta}_i \hat{\theta}_i^3 \\ &+ \bar{z}_i z_{i+1} g_i - \bar{z}_{i-1} z_i g_{i-1} + \frac{a_i^2}{2} + \frac{\epsilon_i^2}{2\underline{g}_i}. \end{aligned} \tag{44}$$

From (35), we have

$$\begin{aligned} \dot{V}_{i-1} \leq &- \sum_{j=1}^{i-1} \frac{b_j \underline{g}_j z_j^4}{(\kappa_j^2 - z_j^2)^2} - \sum_{j=1}^{i-1} \frac{c_j \underline{g}_j z_j^{2p}}{(\kappa_j^2 - z_j^2)^p} + \sum_{j=1}^{i-1} \frac{\eta_j \underline{g}_j}{\mu_j} \tilde{\theta}_j \hat{\theta}_j + \frac{\varkappa_j \underline{g}_j}{\mu_j^2} \tilde{\theta}_j \hat{\theta}_j^3 \\ &+ \bar{z}_{j-1} z_j g_j + \sum_{j=1}^{i-1} \left(\frac{a_j^2}{2} + \frac{\epsilon_j^2}{2\underline{g}_j}\right). \end{aligned} \tag{45}$$

From (44) and (45), we have

$$\begin{aligned} \dot{V}_i \leq &- \sum_{j=1}^{i} \frac{b_j \underline{g}_j z_j^4}{(\kappa_j^2 - z_j^2)^2} - \sum_{j=1}^{i} \frac{c_j \underline{g}_j z_j^{2p}}{(\kappa_j^2 - z_j^2)^p} + \sum_{j=1}^{i} \frac{\eta_j \underline{g}_j}{\mu_j} \tilde{\theta}_j \hat{\theta}_j + \sum_{j=1}^{i} \frac{\varkappa_j \underline{g}_j}{\mu_j^2} \tilde{\theta}_j \hat{\theta}_j^3 \\ &+ \bar{z}_i z_{i+1} \underline{g}_i + \sum_{j=1}^{i} \left(\frac{a_j^2}{2} + \frac{\epsilon_j^2}{2\varphi_j}\right). \end{aligned} \tag{46}$$

Step n: From (1) and (9), we have

$$\begin{aligned} \dot{z}_n &= g_n \zeta_{n+1} + f_n - \dot{\alpha}_{n-1} \\ &= g_n u + f_n - \dot{\alpha}_{n-1} \\ &= g_n (h(v) + p(v)) + f_n - \dot{\alpha}_{n-1} \end{aligned} \tag{47}$$

The BLF V_n is chosen:

$$V_n = V_{n-1} + \frac{1}{2} \log \frac{\kappa_n^2}{\kappa_n^2 - z_n^2} + \frac{\underline{g}_n}{2\mu_n} \tilde{\theta}_n^2 \tag{48}$$

where $\kappa_n > |z_n|$, $\mu_n > 0$, $\tilde{\theta}_n = \theta_n - \hat{\theta}_n$, and $\hat{\theta}_n$ is the estimation of θ_n.

Obviously, V_n is

$$\dot{V}_n = \dot{V}_{n-1} + \bar{z}_n \left(g_n (h(v) + p(v)) + \bar{f}_n(Z_n)\right) - \frac{\underline{g}_n}{\mu_n} \tilde{\theta}_n \dot{\hat{\theta}}_n - \bar{z}_{n-1} g_{n-1} z_n \tag{49}$$

The event-triggered mechanism is formulated based on $m(t)$ defined in (3) as

$$\begin{cases} u(t) = \omega(t_k), \forall t \in [t_k, t_{k+1}) \\ t_{k+1} = \inf\{t \in \mathbb{R} \mid |m(t)| \geq \rho|u(t)| + m_1\} \end{cases} \tag{50}$$

where $0 < \rho < 1$ and $m_1 > 0$ are constants to be specified. Whenever condition (49) is satisfied, we mark this time as t_{k+1} and apply the control value $u(t_{k+1})$ to the system (1). For $t \in [t_k, t_{k+1})$, the control signal remains constant at $\omega(t_k)$.

(50) introduces two time-dependent parameters, $\lambda_i(t)$ for $i = 1, 2$, which satisfy $|\lambda_i(t)| \leq 1$, such that

$$u(t) = \frac{\omega(t) - \lambda_1(t)m_1}{1 + \lambda_2(t)\rho}. \tag{51}$$

Choose the control input

$$\omega(t) = -(1+\rho)\left(\alpha_n \tanh\left(\frac{\bar{z}_n\alpha_n}{\sigma_1}\right) + m_2 \tanh\left(\frac{\bar{z}_n m_2}{\sigma_1}\right)\right) \tag{52}$$

where $m_2 > \frac{m_1}{1-\rho}$ and α_n is the virtual controller design to be later.

It follows that

$$\begin{aligned} \bar{z}_n u = -\bar{z}_n \\ \left(\tfrac{1+\rho}{1+\rho\lambda_2(t)}\left(\alpha_n \tanh\left(\tfrac{\bar{z}_n\alpha_n}{\sigma_1}\right) + m_2 \tanh\left(\tfrac{\bar{z}_n m_2}{\sigma_1}\right)\right) + \tfrac{m_1\lambda 1(t)}{1+\rho\lambda_2(t)}\right). \end{aligned} \tag{53}$$

From Lemma 2, one has

$$\begin{aligned} \bar{z}_n u &\leq |\bar{z}_n\alpha_n| - \bar{z}_n\alpha_n \tanh\left(\frac{\bar{z}_n\alpha_n}{\sigma_1}\right) + |\bar{z}_n m_2| - \bar{z}_n m_2 \tanh\left(\frac{\bar{z}_n m_2}{\sigma_1}\right) - |\bar{z}_n\alpha_n| \\ &\leq \bar{z}_n\alpha_n + 0.557\sigma_1. \end{aligned} \tag{54}$$

Thus, (49) can be written as

$$\dot{V}_n \leq \dot{V}_{n-1} + \bar{z}_n\left(g_n\alpha_n + \bar{f}_n(Z_n)\right) - \frac{\underline{g}_n}{\mu_n}\tilde{\theta}_n\dot{\hat{\theta}}_n - \bar{z}_{n-1}g_{n-1}z_n + 0.557\sigma_1\bar{g}_n \tag{55}$$

where $\bar{z}_n = \frac{z_n}{\kappa_n^2 - z_n^2}$,

$\bar{f}_n(Z_n) = f_n + \bar{z}_{n-1}g_{n-1}(\kappa_n^2 - z_n^2) - \dot{\alpha}_{n-1}$,

$Z_n = [\zeta_1, \ldots, \zeta_n, y_d, \ldots, y_d^{(n-1)}, \hat{\varphi}_1, \ldots, \hat{\theta}_{n-1}]^T$.

Since $\bar{f}_n(Z_n)$ contains the unknown smooth function f_n, then RBFNN $W_n^{*T}S_n(Z_n)$ is applied to model $\bar{f}_n(Z_n)$ such that for any constant $\epsilon_n > 0$:

$$\bar{f}_n(Z_n) = W_n^T S_n(Z_n) + \delta_n(Z_n), \quad |\delta_n(Z_n)| \leq \epsilon_n. \tag{56}$$

By applying Lemma 7 and using the method of completing the square, one has

$$\begin{aligned} \bar{f}_n(Z_n) &= \bar{z}_n\left(W_n^{*T}S_n(Z_n) + \delta_n(Z_n)\right) \\ &\leq |\bar{z}_n|\left(\|W_n^*\|\|S_n(Z_n)\| + \epsilon_n\right) \\ &\leq |\bar{z}_n|\left(\|W_n^*\|\|S_n(Z_n)\| + \epsilon_n\right) \\ &\leq \frac{1}{2a_n^2}\bar{z}_n^2\theta_n\underline{g}_n S_n^T(X_n)S_n(X_n) + \frac{a_n^2}{2} + \frac{\bar{z}_n^2\underline{g}_n}{2} + \frac{\epsilon_n^2}{2\underline{g}_n}, \end{aligned} \tag{57}$$

where $a_n > 0$ is a design parameter, and $\theta_n = \|W_n^*\|^2/\underline{g}_n$, $X_n = Z_n$

Based on (9) and using Young's inequality, we have

$$\bar{z}_n g_n p(v) \leq \frac{1}{2}\bar{z}_n^2 + \frac{1}{2}\underline{g}_n^2 P^2 \tag{58}$$

By using (57) and (58) in (55) gives

$$\begin{aligned} \dot{V}_n \leq \dot{V}_{n-1} &+ \bar{z}_n\left(g_n\alpha_n + \frac{\bar{z}_n\hat{\theta}_n\underline{g}_n S_n^T(X_n)S_n(X_n)}{2a_n^2} + \frac{\bar{z}_n\underline{g}_n}{2}\right) \\ &- \frac{\underline{g}_n}{\mu_n}\tilde{\theta}_n\left(\dot{\hat{\theta}}_n - \frac{\bar{z}_n^2 S_n^T(X_n)S_n(X_n)\mu_n}{2a_n^2}\right) \\ &- \bar{z}_{n-1}z_n g_{n-1} + \frac{a_n^2}{2} + \frac{\epsilon_n^2}{2\underline{g}_n} + 0.557\sigma_1\bar{g}_n + \frac{1}{2}\underline{g}_n^2 P^2. \end{aligned} \tag{59}$$

Next, the virtual control signal α_n and the adaptive law $\hat{\theta}_n$ are formulated as follows:

$$\alpha_n = -\frac{b_n z_n^3}{\kappa_n^2 - z_n^2} - \frac{c_n z^{2p-1}}{(\kappa_n^2 - z_n^2)^{p-1}} - \frac{\bar{z}_n\hat{\theta}_n S_n^T(X_n)S_n(X_n)}{2a_n^2} - \frac{\bar{z}_n^2}{2}, \tag{60}$$

$$\dot{\hat{\theta}}_n = \frac{\bar{z}_n^2 S_n^T(X_n)S_n(X_n)\mu_n}{2a_n^2} - \eta_n\hat{\theta}_n - \frac{\varkappa_n}{\mu_n}\hat{\theta}_n^3 \tag{61}$$

where $b_n > 0$, $p \in \left(\frac{1}{2}, 1\right)$, $c_n > 0$, $\varkappa_n > 0$, and $\eta_n > 0$ represent the design parameters.

By using (60) and (61) into (59), one has

$$\begin{aligned} \dot{V}_n &\leq \dot{V}_{n-1} - \frac{b_n\underline{g}_n z_n^4}{(\kappa_n^2 - z_n^2)^2} - \frac{c_n\underline{g}_n z_n^{2p}}{(\kappa_n^2 - z_n^2)^p} + \\ &\frac{\eta_n\underline{g}_n}{\mu_n}\tilde{\theta}_n\hat{\theta}_n + \frac{\varkappa_n\underline{g}_n}{\mu_n^2}\tilde{\theta}_n\hat{\theta}_n^3 - \bar{z}_{n-1}z_n g_{n-1} + \frac{a_n^2}{2} \\ &+ \frac{\epsilon_n^2}{2\underline{g}_n} + 0.557\sigma_1\bar{g}_n + \frac{1}{2}\underline{g}_n^2 P^2 \\ &\leq -\sum_{j=1}^{n}\frac{b_j\underline{g}_j z_j^4}{(\kappa_j^2 - z_j^2)^2} - \sum_{j=1}^{n}\frac{c_j\underline{g}_j z_j^{2p}}{(\kappa_j^2 - z_j^2)^p} + \sum_{j=1}^{n}\frac{\eta_j\underline{g}_j}{\mu_j}\tilde{\theta}_j\hat{\theta}_j + \\ &\sum_{j=1}^{n}\frac{\varkappa_j\underline{g}_j}{\mu_j^2}\tilde{\theta}_j\hat{\theta}_j^3 \quad + \sum_{j=1}^{n}\left(\frac{a_j^2}{2} + \frac{\epsilon_j^2}{2\underline{g}_j}\right) + \\ &0.557\sigma_1\bar{g}_n + \frac{1}{2}\underline{g}_n^2 P^2. \end{aligned} \tag{62}$$

By using Young's inequality, one has

$$\frac{\eta_j\underline{g}_j}{\mu_j}\tilde{\theta}_j\hat{\theta}_j \leq -\frac{\eta_j\underline{g}_j}{2\mu_j}\tilde{\theta}_j^2 + \frac{\eta_j\underline{g}_j}{2\mu_j}\hat{\theta}_j^2. \tag{63}$$

Additionally, according to Lemma 5, by defining $\iota = (1-p)p^{\frac{p}{1-p}}$, $b_1 = 1-p$, $b_2 = p$, $x = 1$, $x = \sum_{j=1}^{n}\frac{\eta_j\underline{g}_j}{2\mu_j}\tilde{\theta}_j^2$, and $b_3 = p^{\frac{p}{1-p}}$, we obtain

$$\left(\sum_{j=1}^{n}\frac{\eta_j\underline{g}_j}{2\mu_j}\tilde{\theta}_j^2\right)^p \le \iota+\sum_{j=1}^{n}\frac{\eta_j\underline{g}_j}{2\mu_j}\tilde{\theta}_j^2. \tag{64}$$

By using (63) and (64) into (62) gives

$$\begin{aligned}\dot{V}_n \le& -\sum_{j=1}^{n}\frac{b_j\underline{g}_j z_j^4}{(\kappa_j^2-z_j^2)^2}-\sum_{j=1}^{n}\frac{c_j\underline{g}_j z_j^{2p}}{(\kappa_j^2-z_j^2)^p}-\left(\sum_{j=1}^{n}\frac{\eta_j\underline{g}_j}{2\mu_j}\tilde{\theta}_j^2\right)^p+\sum_{j=1}^{n}\frac{\varkappa_j\underline{g}_j}{\mu_j^2}\tilde{\theta}_j\hat{\theta}_j^3\\&+\sum_{j=1}^{n}\left(\frac{\eta_j\underline{g}_j}{2\mu_j}\tilde{\theta}_j^2+\frac{a_j^2}{2}+\frac{\epsilon_j^2}{2\underline{g}_j}\right)+\iota+0.557\sigma_1\bar{g}_n+\frac{1}{2}\underline{g}_n^2P^2.\end{aligned} \tag{65}$$

By Young's inequality, one has

$$\frac{\varkappa_j\underline{g}_j}{\mu_j^2}\tilde{\theta}_j\hat{\theta}_j^3=\frac{\varkappa_j\underline{g}_j}{\mu_j^2}\tilde{\theta}_j(\theta_j^3+3\theta_j\tilde{\theta}_j^2-3\theta_j^2\tilde{\theta}_j-\tilde{\theta}_j^3). \tag{66}$$

Furthermore, we have

$$\tilde{\theta}_j\theta_j^3\le\frac{\theta_j^4}{12}+3\theta_j^2\tilde{\theta}_j^2, \tag{67}$$

$$3\tilde{\theta}_j^3\theta_j\le\frac{9\tau_j^{4/3}\tilde{\theta}_j^4}{4}+\frac{3\theta_j^4}{4\tau_j^4}, \tag{68}$$

where $\tau_j>0$.

From (66)–(68), we have

$$\frac{\varkappa_j\underline{g}_j}{\mu_j^2}\tilde{\theta}_j\hat{\theta}_j^3\le-\frac{4\varkappa_j-9\zeta_j\tau_j^{3/4}}{\underline{g}_j}\left(\frac{\underline{g}_j}{2\mu_j}\tilde{\theta}_j^2\right)^2+\frac{\varkappa_j\underline{g}_j\theta_j^4}{12\mu_j^2}+\frac{3\varkappa_j\underline{g}_j\theta_j^4}{4\tau_j^4\mu_j^2}. \tag{69}$$

By using (69)–(65), we have

$$\begin{aligned}\dot{V}_n\le&-\sum_{j=1}^{n}\frac{b_j\underline{g}_j z_j^4}{(\kappa_j^2-z_j^2)^2}-\sum_{j=1}^{n}\frac{c_j\underline{g}_j z_j^{2p}}{(\kappa_j^2-z_j^2)^p}-\sum_{j=1}^{n}\frac{4\varkappa_j-9\zeta_j\tau_j^{3/4}}{\underline{g}_j}\left(\frac{\underline{g}_j}{2\mu_j}\tilde{\theta}_j^2\right)^2\\&-\left(\sum_{j=1}^{n}\frac{\eta_j\underline{g}_j}{2\mu_j}\tilde{\theta}_j^2\right)^p+\sigma_2,\end{aligned} \tag{70}$$

where

$$\begin{aligned}\sigma_2=&\sum_{j=1}^{n}\left(\frac{\eta_j\underline{g}_j}{2\mu_j}\theta_j^2+\frac{a_j^2}{2}+\frac{\epsilon_j^2}{2\underline{g}_j}+\frac{\varkappa_j\underline{g}_j\theta_j^4}{12\mu_j^2}+\frac{3\varkappa_j\underline{g}_j\theta_j^4}{4\tau_j^4\mu_j^2}\right)\\&+\iota+0.557\sigma_1\bar{g}_n+\frac{1}{2}\underline{g}_n^2P^2.\end{aligned} \tag{71}$$

Thus, by using Lemma 1 and Lemma 6, we have

$$\begin{aligned}\dot{V}_n\le&-a_0\left(\sum_{j=1}^{n}\frac{1}{2}\log\frac{\kappa_j^2}{\kappa_j^2-z_j^2}\right)^2-\varrho_1\left(\sum_{j=1}^{n}\frac{1}{2}\log\frac{\kappa_j^2}{\kappa_j^2-z_j^2}\right)^p\\&-b_0\left(\sum_{j=1}^{n}\frac{\underline{g}_j}{2\mu_j}\tilde{\theta}_j^2\right)^2-\varrho_2\left(\sum_{j=1}^{n}\frac{\underline{g}_j}{2\mu_j}\tilde{\theta}_j^2\right)^p+\sigma_2,\end{aligned} \tag{72}$$

where

$$a_0=\frac{4\min\{b_1\underline{g}_1,b_2\underline{g}_2,\ldots,b_n\underline{g}_n\}}{n}, \tag{73}$$

$$\varrho_1=2p\min\{c_1\underline{g}_1,c_2\underline{g}_2,\ldots,c_n\underline{g}_n\}, \tag{74}$$

$$\varrho_2=\min\{\eta_1^p,\eta_2^p,\ldots,\eta_n^p\}, \tag{75}$$

$$b_0=\frac{\min\left\{\frac{4\varkappa_1-9\varkappa_1\tau_1^{4/3}}{\underline{g}_1},\frac{4\varkappa_2-9\varkappa_2\tau_2^{4/3}}{\underline{g}_2},\ldots,\frac{4\varkappa_n-9\varkappa_n\tau_n^{4/3}}{\underline{g}_n}\right\}}{n}. \tag{76}$$

Furthermore, we have

$$\dot{V}_n\le-\varsigma V_n^2-\varrho V_n^p+\sigma_2, \tag{77}$$

where

$$\varsigma=\frac{\min\{a_0,b_0\}}{2},\quad \varrho=\min\{\varrho_1,\varrho_2\}. \tag{78}$$

Theorem 1 *For the system (1) under Assumptions 1–4, the proposed control strategy ensures that all signals remain bounded and the tracking error converges to a region near the origin within a fixed time. Moreover, this method avoids Zeno behavior.*

Proof Based on Inequality (77) and Lemma 3, the error system (26) can converge to the set defined by

$$\Omega=\left\{X\mid V_n(X)\le\min\left\{\left(\frac{\sigma_2}{\varsigma(1-\pi)}\right)^{\frac{1}{2}},\left(\frac{\sigma_2}{\varrho(1-\pi)}\right)^{\frac{1}{p}}\right\}\right\}, \tag{79}$$

where $X=[z_1,z_2,\ldots,z_n,\tilde{\theta}_1,\tilde{\theta}_2,\ldots,\tilde{\theta}_n]^T$.

Furthermore, the settling time is determined by

$$T_s\le\frac{1}{\varsigma\pi}+\frac{1}{\varrho\pi(1-p)}. \tag{80}$$

Referring to the definition of V_n, it becomes evident that for $t\ge T_s$, one can straightforwardly derive

$$z_i\le\min\left\{\left(\frac{4\sigma_2}{\varsigma(1-\pi)}\right)^{\frac{1}{4}},\left(\frac{2p\sigma_2}{\varrho(1-\pi)}\right)^{\frac{1}{2p}}\right\}, \tag{81}$$

and

$$\tilde{\theta}_i\le\min\left\{\left(\frac{4\sigma_2}{\varsigma(1-\pi)}\right)^{\frac{1}{4}},\left(\frac{2p\sigma_2}{\varrho(1-\pi)}\right)^{\frac{1}{2p}}\right\}. \tag{82}$$

Therefore, the signals z_i and $\tilde{\theta}_i$ remain bounded. Considering that $\tilde{\theta}_i = \theta_i - \hat{\theta}_i$ and acknowledging that θ_i is bounded, it implies that $\hat{\theta}_i$ must also be bounded. Referring to (26) and the bounded nature of y_d, it can be deduced that ζ_1 is also bounded. As a result, the virtual control signal α_1, along with $u(t)$ and $\omega(t)$, are also bounded.

Since $|y_d| \leq Y_0$ and $z_1 \leq \kappa_1$, it follows that $|\zeta_1| \leq \kappa_1 + Y_0 = \bar{\kappa}_1$. Moreover, given that $z_i = x_i - \alpha_{i-1}$ and $z_i \leq \kappa_i$, we find $\zeta_i \leq \kappa_i + \bar{\alpha}_{i-1} = \bar{\kappa}_i$, where $|\alpha_{i-1}| \leq \bar{\alpha}_{i-1}$ for $i = 2, 3, \ldots, n$. Consequently, the system states adhere to their specified constraints. As per (52), the control signal $\omega(t)$ comprises bounded signals such as α_n, $\bar{z}_n$, g_n, ρ, m_2, and σ_1. Thus, $\omega(t)$ is bounded, meaning there exists a positive constant $\bar{\omega}$ such that $|\dot{\omega}(t)| \leq \bar{\omega}$. Additionally, we have $m(t_k) = 0$ and $\lim_{t \to t_{k+1}} m(t) = \rho|u(t)| + m_1$.

To prove that Zeno behavior is avoided, consider the triggering instants $\{t_k\}$ and define the measurement error as

$$m(t) = \omega(t) - u(t), \quad m(t_k) = 0. \tag{83}$$

The event-triggering condition is given by

$$|m(t)| \geq \rho|u(t)| + m_1, \tag{84}$$

where $m_1 > 0$ is a strictly positive constant, ensuring that a nonzero threshold must be reached before the next triggering event. The control signal $\omega(t)$ is composed of bounded terms, which implies the existence of a positive constant $\bar{\omega}$ such that

$$|\dot{\omega}(t)| \leq \bar{\omega}, \quad \forall t \in [t_k, t_{k+1}). \tag{85}$$

Consequently, the rate of change of the measurement error satisfies

$$\frac{d|m(t)|}{dt} = \text{sgn}(m(t))\dot{m}(t) \leq |\dot{\omega}(t)| \leq \bar{\omega}, \quad \forall t \in [t_k, t_{k+1}). \tag{86}$$

Starting from $m(t_k) = 0$, the time required for the error to reach the threshold $\rho|u(t)| + m_1$ is strictly positive and can be lower bounded as

$$t_{k+1} - t_k \geq \frac{\rho|u(t)| + m_1}{\bar{\omega}} > 0. \tag{87}$$

Since the inter-event interval is strictly positive, the triggering instants cannot accumulate in finite time. This ensures that Zeno behavior is effectively avoided under the proposed event-triggered control framework. □

To better illustrate the control procedures, the fixed-time event-triggered control scheme is presented in Fig. 1.

Remark 4 According to (77), the proposed controller ensures that the tracking errors converge to adjustable small neighborhoods around zero within a fixed time. The design parameters b_i and c_i $(i = 1, 2, \ldots, n)$ are first selected to satisfy the fixed-time stability conditions obtained from the Lyapunov analysis, which mainly affect the convergence speed and the settling time. The parameters $\varkappa_i$ and η_i influence the size of the ultimate tracking error bounds and the control effort. In practice, these parameters are chosen using a trial-and-error procedure by observing the closed-loop system performance, such as tracking accuracy and control magnitude. Starting from moderate positive values that meet the theoretical conditions, the parameters are gradually

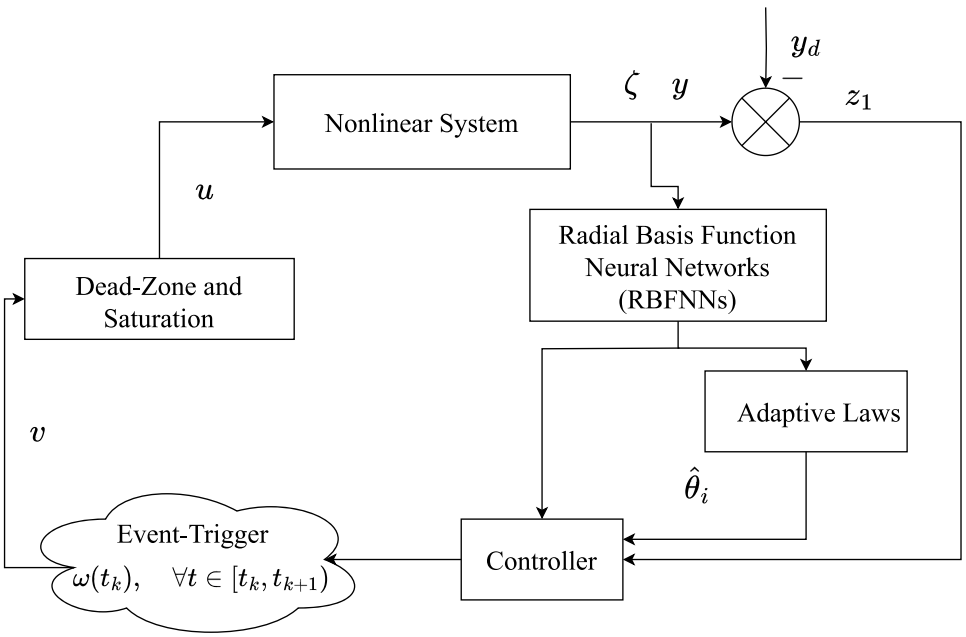

Fig. 1 The block diagram of control scheme

adjusted to achieve a balance between satisfactory tracking performance and feasible control input.

Remark 5 In this work, constant full-state constraints are handled using a barrier Lyapunov function that enforces constraint satisfaction throughout the system evolution. The barrier Lyapunov function increases rapidly as the state approaches the constraint boundary, which prevents constraint violation at all times. At the same time, the controller design ensures that the time derivative of the barrier Lyapunov function satisfies a fixed-time stability condition with appropriately selected positive design parameters. As a result, the tracking errors converge to a small neighborhood of the origin within a fixed time that does not depend on the initial conditions, while all state variables remain strictly inside their prescribed constant bounds. This shows that the barrier Lyapunov function naturally integrates with the fixed-time stability framework and does not conflict with the fixed-time convergence property.

4 Simulation results

In this section, the efficacy and benefits of the proposed method are demonstrated through a numerical example and a practical application involving a pendulum system.

Example 1 Consider the following second-order nonlinear system:

$$\begin{cases} \dot{\zeta}_1 = (2+\sin(\zeta_1))\zeta_2 + 0.1\sin(\zeta_1\zeta_2) \\ \dot{\zeta}_2 = (2+\cos(\zeta_1\zeta_2))u + 0.5\sin(\zeta_1^2\zeta_2^2) \\ y = \zeta_1 \end{cases} \tag{88}$$

where ζ_1 and ζ_2 represent the state variables, and u and y denote the input and output signals, respectively. Here, $g_1(\zeta_1) = 2+\sin(\zeta_1)$, $g_2(\zeta_2) = 2+\cos(\zeta_1\zeta_2)$, $f_1 = 0.1\sin(\zeta_1\zeta_2)$, and $f_2 = 0.5\sin(\zeta_1^2\zeta_2^2)$. The state constraints are specified as $|\zeta_1| \le 1$ and $|\zeta_2| \le 2$. Additionally, the reference signal is given by $y_d(t) = 0.5\sin(t)$.

Design the virtual controller as

$$\alpha_1 = -\frac{b_1 z_1^3}{\kappa_1^2 - z_1^2} - \frac{c_1 z^{2p-1}}{(\kappa_1^2 - z_1^2)^{p-1}} - \frac{\bar{z}_1\hat{\theta}_1 S_1^T(X_1)S_1(X_1)}{2a_1^2} - \frac{\bar{z}_1^2}{2}, \tag{89}$$

Design the relative-threshold-based control signal as follows:

$$\omega(t) = -(1+\rho)\left(\alpha_2\tanh\left(\frac{\bar{z}_2\alpha_2}{\sigma_1}\right) + m_2\tanh\left(\frac{\bar{z}_2 m_2}{\sigma_1}\right)\right) \tag{90}$$

with the triggering mechanism

$$\begin{cases} u(t) = \omega(t_k), \forall t \in [t_k, t_{k+1}) \\ t_{k+1} = \inf\{t \in \mathbb{R} \mid |m(t)| \ge \rho|u(t)| + m_1\} \end{cases} \tag{91}$$

Design adaptive law as follows

$$\dot{\hat{\theta}}_i = \frac{\bar{z}_i^2 S_i^T(X_i)S_i(X_i)\mu_i}{2a_i^2} - \eta_i\hat{\theta}_i - \frac{\varkappa_i}{\mu_i}\hat{\theta}_i^3, \quad i = 1,2 \tag{92}$$

The design parameters are specified as follows: $p = \frac{4}{5}$, $b_1 = c_1 = b_2 = c_2 = 4$, $\kappa_1 = 0.5$, $\kappa_2 = 2$, $a_1 = a_2 = 0.1$, $\mu_1 = \mu_2 = 1$, $\eta_1 = 0.03$, $\eta_2 = 0.01$, $\varkappa = 0.1$, $n_1 = 0.2$, $\sigma_1 = 0.01$, $m_2 = \frac{m_1}{1-\rho} + 0.01$. The initial conditions are set as $[\zeta_1(0), \zeta_2(0), \hat{\theta}_1(0), \hat{\theta}_2(0)]^T = [0.5, 0.5, 0, 0]^T$. Additionally, the neural network $S_1^T(Z_1)S_1(Z_1)$ comprises 49 nodes with centers evenly spaced over the range $[-5,5]\times[-5,5]$ and widths of two. The neural network $S_2^T(Z_2)S_2(Z_2)$ comprises 343 nodes with centers evenly spaced over the range $[-5,5]\times[-5,5]\times[-5,5]$ and widths of two.

Figures 2–7 illustrate the simulation results obtained with the proposed controller. Figure 2 shows the tracking trajectories of the system output $y = \zeta_1$, the reference signal $y_d(t)$, constraint $\bar{\kappa}_1$. It is clear from this figure that the system performs well in tracking, with the state variable ζ_1 staying within its constraint $\bar{\kappa}_1$. Figure 3 depicts the tracking error z_1, which remains bounded. Figure 4 presents the trajectories of the system state ζ_2, demonstrating that ζ_2 also stays within its constraint $\bar{\kappa}_2$. Figure 5 illustrates the trajectories of the adaptive laws $\hat{\theta}_1$ and $\hat{\theta}_2$. Figure 6 shows the control input v and the event-triggered control input ω and system input u. Figure 7 depicts the time intervals of the relative threshold event-triggered mechanism.

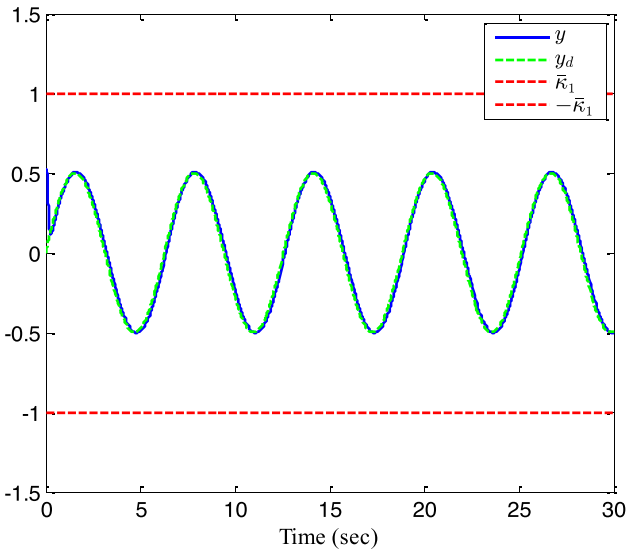

Fig. 2 Trajectories of system output y, reference signal y_d and constraint $\bar{\kappa}_1$

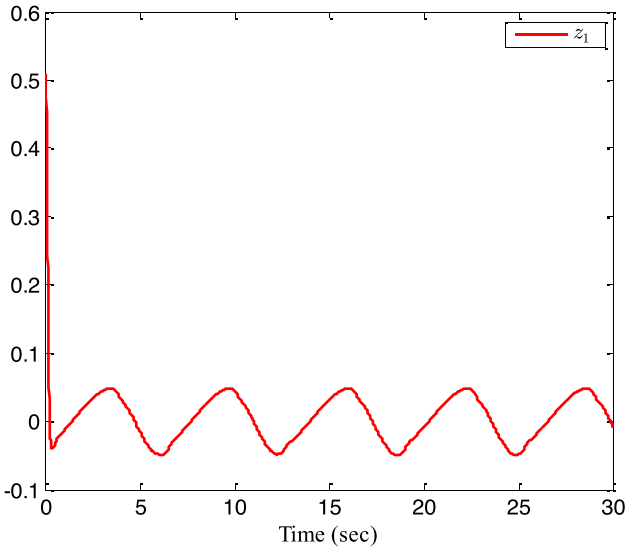

Fig. 3 The response of tracking error z_1

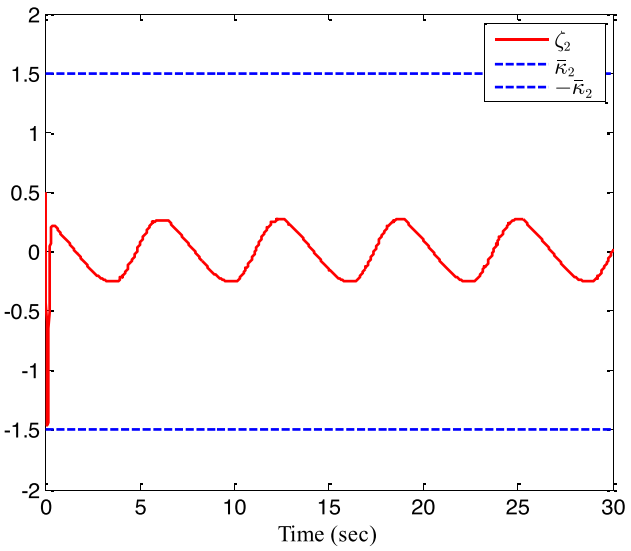

Fig. 4 The curve of state variable ζ_2 and constraint $\bar{\kappa}_2$

Comparative performance analysis: To illustrate the fixed-time property and independence from initial conditions, Example 1 is simulated with three sets of initial states: Case 1: $[\zeta_1(0), \zeta_2(0)]^T = [0.5, 0.5]^T$, Case 2: $[\zeta_1(0), \zeta_2(0)]^T = [1.0, -0.5]^T$, and Case 3: $[\zeta_1(0), \zeta_2(0)]^T = [-0.8, 0.7]^T$. The proposed fixed-time adaptive control method is compared with an existing finite-time control method [32]. In all cases, the system states converge to the desired trajectory within the same fixed time $T_s = 1.2$ s, confirming the theoretical fixed-time stability. The tracking performance is evaluated using standard error metrics. For N samples of the actual output $y(t)$ and desired signal $y_d(t)$, the metrics are defined as

$$\text{MAE} = \max_{1 \le t \le N} |y(t) - y_d(t)|, \tag{93}$$

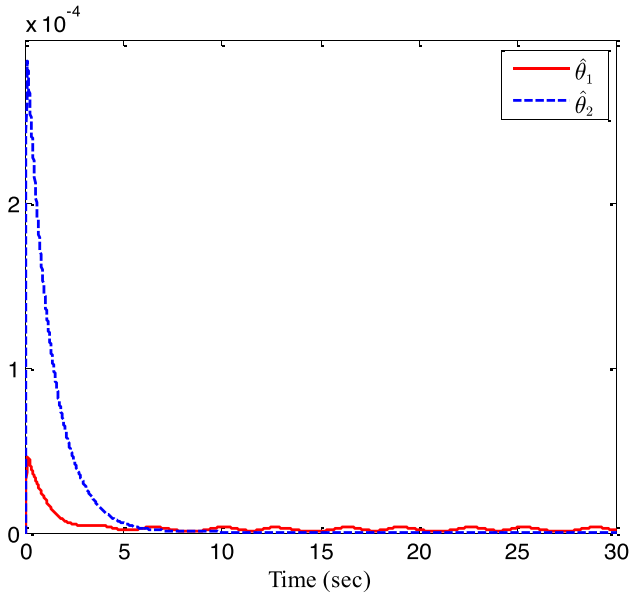

Fig. 5 Adaptive parameters $\hat{\theta}_1$ and $\hat{\theta}_2$

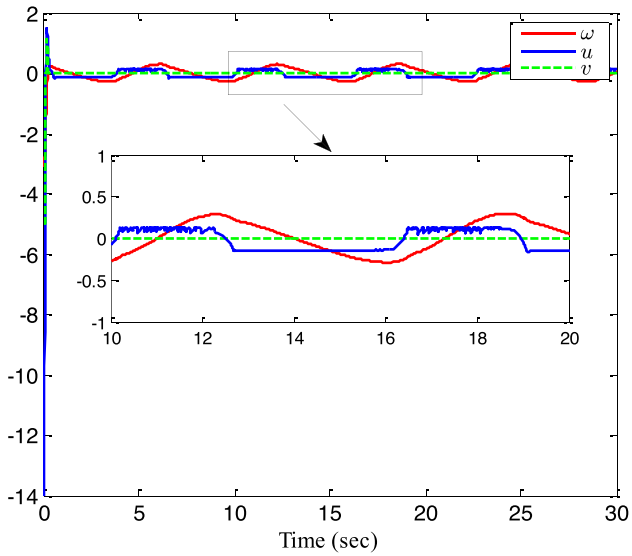

Fig. 6 Control input v and the event-triggered control input ω and system input u

$$\text{SSE} = \sum_{t=1}^{N} \left(y(t) - y_d(t)\right)^2, \tag{94}$$

$$\text{MSE} = \frac{1}{N} \sum_{t=1}^{N} \left(y(t) - y_d(t)\right)^2, \tag{95}$$

$$\text{RMSE} = \sqrt{\text{MSE}}, \tag{96}$$

$$\text{NMSE} = \frac{\sum_{t=1}^{N} \left(y(t) - y_d(t)\right)^2}{\sum_{t=1}^{N} \left(y_d(t) - \bar{y}_d\right)^2}, \tag{97}$$

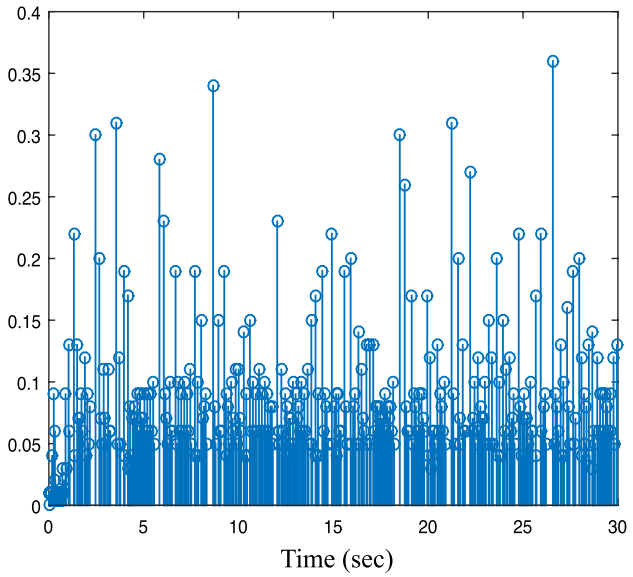

Fig. 7 Time-intervals of triggering events

$$\mathrm{BFR} = \left(1 - \frac{\sqrt{\sum_{t=1}^{N}\left(y(t) - y_d(t)\right)^2}}{\sqrt{\sum_{t=1}^{N}\left(y_d(t) - \bar{y}_d\right)^2}}\right) \times 100\% \tag{98}$$

where $\bar{y}_d = \frac{1}{N}\sum_{t=1}^{N} y_d(t)$ is the mean of the desired signal. Table 1presents the performance of the proposed fixed-time method and the existing finite-time method [32] for the three initial state cases.

Table 1 shows that the proposed fixed-time method consistently outperforms the existing finite-time method across all three initial states. The MAE, SSE, MSE, and RMSE values are smaller for the fixed-time method, indicating more accurate tracking. The NMSE is lower, and the BFR values are higher, confirming better overall performance. Importantly, the system reaches the desired trajectory within the same fixed time $T_s = 1.2$ s for all initial conditions, demonstrating the fixed-time property where settling time is independent of initial states. In contrast, the finite-time method shows slight variations in performance depending on the initial conditions, highlighting the advantage of the proposed fixed-time approach.

Example 2 Consider the pendulum system described in [51]:

$$ML\ddot{\vartheta} + BL\dot{\vartheta} + MgL\sin\vartheta = u, \tag{99}$$

where ϑ is the angle between the rod and the vertical upward direction, and $\dot{\vartheta}$ is the rod's angular velocity. M denotes the mass of the bob, L is the length of the rod, B represents the frictional coefficient, and g is the acceleration due to gravity. The parameters are selected as $M = 0.25\,\mathrm{kg}$, $L = 4\,\mathrm{m}$, $B = 0.25$, and $g = 10\,\mathrm{m/s^2}$.

Then, define $\zeta_1 = \vartheta$ and $\zeta_2 = \dot{\vartheta}$, the pendulum system can be rewritten as:

$$\begin{cases} \dot{\zeta}_1 = \zeta_2, \\ \dot{\zeta}_2 = \frac{1}{ML}u + \left(-\frac{g}{L} - \frac{B}{M}\right)\sin(\zeta_1\zeta_2), \\ y = \zeta_1. \end{cases} \tag{100}$$

The reference signal is chosen as$y_d = 0.2\sin(t) + 0.4\sin(0.3t)$.

Design the virtual controller as

$$\alpha_1 = -\frac{b_1 z_1^3}{\kappa_1^2 - z_1^2} - \frac{c_1 z^{2p-1}}{(\kappa_1^2 - z_1^2)^{p-1}} - \frac{\bar{z}_1\hat{\theta}_1 S_1^T(X_1)S_1(X_1)}{2a_1^2} - \frac{\bar{z}_1^2}{2}, \tag{101}$$

Design the relative-threshold-based control signal as follows:

$$\omega(t) = -(1+\rho)\left(\alpha_2 \tanh\left(\frac{\bar{z}_2\alpha_2}{\sigma_1}\right) + m_2 \tanh\left(\frac{\bar{z}_2 m_2}{\sigma_1}\right)\right) \tag{102}$$

Table 1 Comparative performance of the proposed fixed-time method and an existing finite-time method under different initial conditions

Case / Method	MAE	SSE	MSE	RMSE	NMSE	BFR(%)
Case 1: Initial state $[0.5, 0.5]^T$						
Proposed Fixed-Time	0.048	0.128	0.000043	0.0065	0.00042	99.95
Finite-Time [32]	0.076	0.202	0.000067	0.0082	0.00064	99.88
Case 2: Initial state $[1.0, -0.5]^T$						
Proposed Fixed-Time	0.049	0.130	0.000044	0.0066	0.00043	99.94
Finite-Time [32]	0.080	0.215	0.000071	0.0084	0.00067	99.85
Case 3: Initial state $[-0.8, 0.7]^T$						
Proposed Fixed-Time	0.047	0.127	0.000042	0.0064	0.00041	99.96
Finite-Time [32]	0.083	0.225	0.000074	0.0086	0.00070	99.83

with the triggering mechanism

$$\begin{cases} u(t) = \omega(t_k), \forall t \in [t_k, t_{k+1}) \\ t_{k+1} = \inf\{t \in \mathbb{R} \mid |m(t)| \geq \rho|u(t)| + m_1\} \end{cases} \quad (103)$$

Design adaptive law as follows

$$\dot{\hat{\theta}}_i = \frac{\bar{z}_i^2 S_i^T(X_i) S_i(X_i) \mu_i}{2a_i^2} - \eta_i \hat{\theta}_i - \frac{\varkappa_i}{\mu_i} \hat{\theta}_i^3, \quad i = 1, 2 \quad (104)$$

The design parameters are specified as follows: $p = \frac{4}{5}$, $b_1 = c_1 = b_2 = c_2 = 4$, $\kappa_1 = 0.5$, $\kappa_2 = 2$, $a_1 = a_2 = 0.1$, $\mu_1 = \mu_2 = 1$,$\eta_1 = \zeta_1 = 0.03$,$\eta_2 = \zeta_2 = 0.01$,$\rho = 0.1$,$m_1 = 0.2$, $\sigma_1 = 0.01$, $m_2 = \frac{m_1}{1-\rho} + 0.01$. The initial conditions are set as $[\zeta_1(0), \zeta_2(0), \hat{\theta}_1(0), \hat{\theta}_2(0)]^T = [0.5, 0.5, 0, 0]^T$. Additionally, the neural network $S_1^T(Z_1)S_1(Z_1)$ contains 49 nodes with centers evenly distributed in the range $[-5, 5] \times [-5, 5]$ and widths of two. The neural network $S_2^T(Z_2)S_2(Z_2)$ contains 343 nodes with centers evenly distributed in the range $[-5, 5] \times [-5, 5] \times [-5, 5]$ and widths of two.

Figures 8–13 illustrate the simulation results obtained with the proposed controller. Figure 8 shows the tracking trajectories of the system output $y = \zeta_1$, the reference signal $y_d(t)$, and constraint $\bar{\kappa}_1$. It is evident from this figure that the system exhibits effective tracking performance, with the state variable ζ_1 remaining within its specified constraint $\bar{\kappa}_1$. Figure 9 depicts the tracking error z_1, which remains bounded. Figure 10 presents the trajectories of the system state ζ_2, demonstrating that ζ_2 also adheres to its constraints $\bar{\kappa}_2$. Figure 11 illustrates the trajectories of the adaptive laws $\hat{\theta}_1$ and $\hat{\theta}_2$. Figure 12 shows the shows the control input v and the event-triggered control input ω and system input u. Figure 13 depicts the time intervals of the relative threshold event-triggered mechanism.

Comparative performance analysis: To demonstrate the fixed-time property and independence from initial conditions, the system is simulated under three different sets of initial states: Case 1: $[\zeta_1(0), \zeta_2(0)]^T = [0.5, 0.5]^T$, Case 2: $[\zeta_1(0), \zeta_2(0)]^T = [1.0, -0.5]^T$, and Case 3: $[\zeta_1(0), \zeta_2(0)]^T = [-0.8, 0.7]^T$. The proposed fixed-time adaptive control method is compared with the existing finite-time method [32]. In all cases, the system states converge to the desired trajectory within the same fixed time $T_s = 1.5$ s, confirming the theoretical fixed-time stability. Table 2 summarizes the performance of the proposed fixed-time method and the existing finite-time method [32] for the three initial state cases.

Table 2 demonstrates that the proposed fixed-time method maintains superior tracking performance under actuator faults and disturbances for all three initial conditions. The MAE, SSE, MSE, and RMSE values are consistently lower than the finite-time method, and the BFR is higher. The system reaches the desired trajectory within the same fixed time $T_s = 1.5$ s regardless of the initial states, confirming the fixed-time property and robustness against uncertainties. In contrast, the finite-time method shows slight variations in convergence and performance metrics depending on the initial conditions.

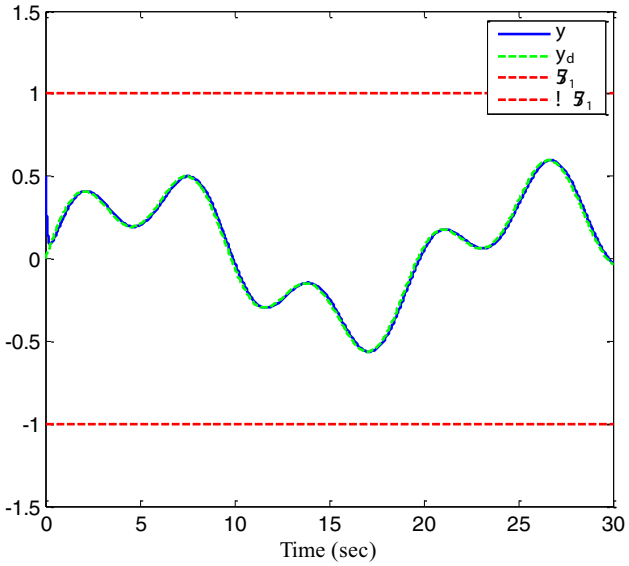

Fig. 8 Trajectories of system output y, reference signal y_d and constraint $\bar{\kappa}_1$

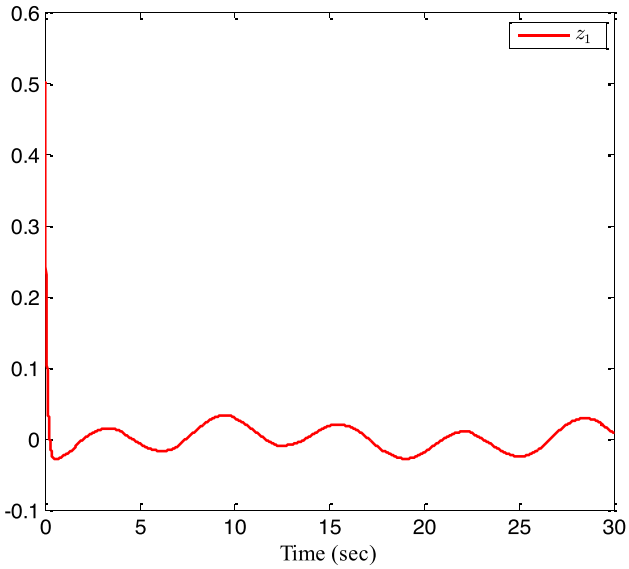

Fig. 9 The response of tracking error z_1

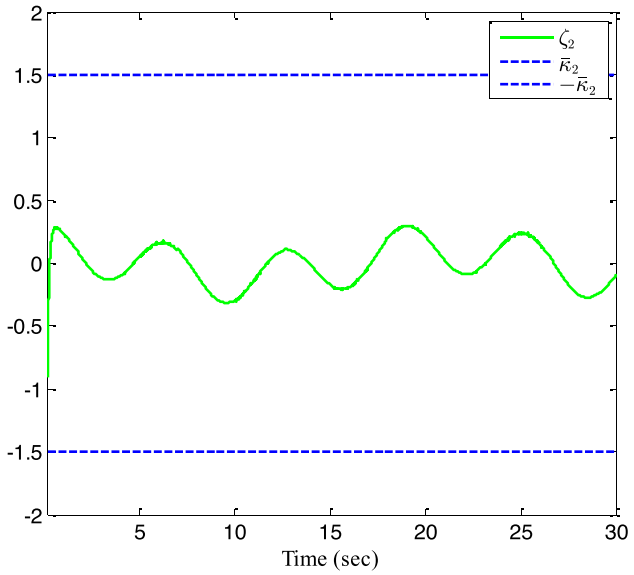

Fig. 10 The curve of state variable ζ_2 and constraint $\bar{\kappa}_2$

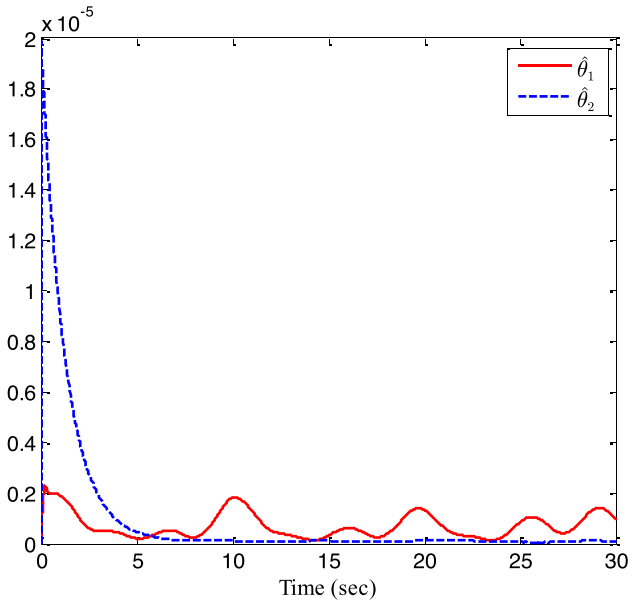

Fig. 11 Adaptive parameters $\hat{\theta}_1$ and $\hat{\theta}_2$

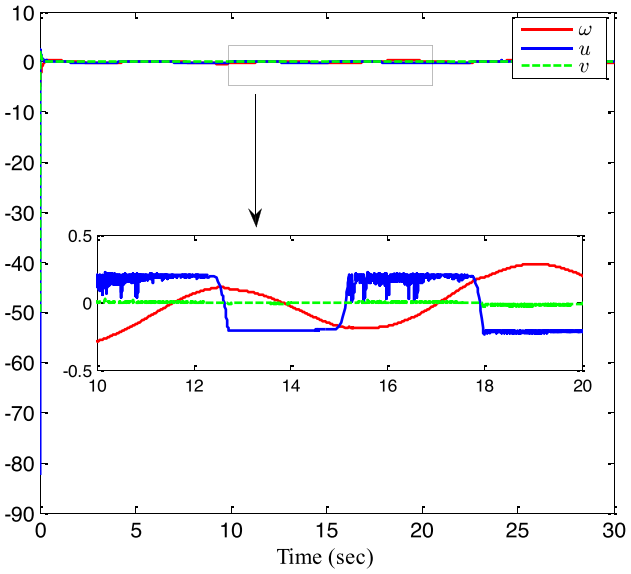

Fig. 12 Control input v and the event-triggered control input ω and system input u

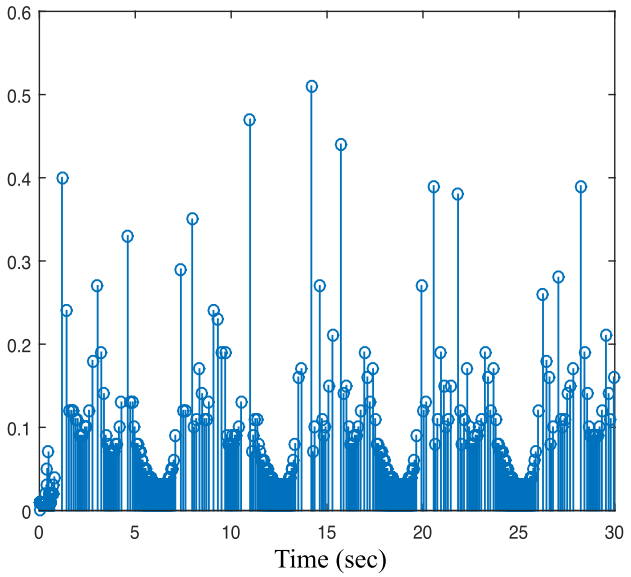

Fig. 13 Time-intervals of triggering events

5 Conclusion

This paper presents a fixed-time neural adaptive event-triggered control approach for nonstrict-feedback nonlinear systems with full-state constraints, input dead-zone, and saturation. Utilizing RBFNNs to address unknown nonlinearities, the method approximates non-smooth effects and transforms them into an affine form. By integrating backstepping design with a varying threshold event-triggered condition, the proposed algorithm uses BLFs and RBFNNs to ensure that the tracking error converges within a fixed time and all closed-loop variables remain bounded. The effectiveness of the method is demonstrated through two simulation examples. In future work, the proposed

Table 2 Comparative performance of the proposed fixed-time method and an existing finite-time method under different initial conditions

Case / Method	MAE	SSE	MSE	RMSE	NMSE	BFR(%)
Case 1: Initial state $[0.5, 0.5]^T$						
Proposed Fixed-Time	0.063	0.186	0.000062	0.0079	0.00059	99.93
Finite-Time [32]	0.102	0.290	0.000095	0.0097	0.00075	99.86
Case 2: Initial state $[1.0, -0.5]^T$						
Proposed Fixed-Time	0.065	0.190	0.000064	0.0080	0.00061	99.92
Finite-Time [32]	0.110	0.310	0.000102	0.0101	0.00082	99.83
Case 3: Initial state $[-0.8, 0.7]^T$						
Proposed Fixed-Time	0.061	0.180	0.000060	0.0077	0.00057	99.94
Finite-Time [32]	0.115	0.325	0.000108	0.0104	0.00088	99.81

adaptive fixed-time event-triggered control strategy will be extended to more complex nonlinear systems, including robotic manipulators and industrial process control applications. Practical factors such as sensor noise, actuator dynamic delays, and other uncertainties will be considered to enhance the robustness and real-world applicability of the control approach. Furthermore, strategies to reduce computational complexity, optimize neural network structures, and provide systematic tuning guidelines for design parameters will be investigated to facilitate practical implementation.

Author Contributions Mohamed Kharrat: Writing – original draft, Supervision, Paolo Mercorelli: Writing – review & editing.

Funding Open Access funding enabled and organized by Projekt DEAL.

Data Availability No datasets were generated or analysed during the current study.

Declarations

Conflicts of Interest The authors declare that there are no conflicts of interest.

References

1. Raza MA, Agama FT, Sultana S, Rashid S, Alsubaie AS (2025) Elagan SK (2025) Exploring the influencing factors on stochastic codynamics for nonlinear fractional epidemic model with control strategies. Adv Contin Discrete Models 1:129
2. Kharrat M (2024) Neural networks-based adaptive fault-tolerant control for stochastic nonlinear systems with unknown backlash-like hysteresis and actuator faults. J Appl Math Comput 70(3):1995–2018
3. Kharrat M (2024) Adaptive fault-tolerant control for a class of nonstrict-feedback nonlinear systems with unmodeled dynamics and dead-zone output using multi-dimensional taylor networks. Non Dyn pp 1–18
4. Liu X, Shi X (2019) Li, Y (2019) Neural networks-based adaptive finite-time control of switched nonlinear systems under time-varying actuator failures. Adv Diff Equ 1:482
5. Trigunarsyah B, Laksono NB (2025) Fuzzy Bayesian Belief Networks Method on Risk Assessment of EPC Pipeline Project. Civil Eng J (Iran) 11(3):1050–1071
6. Trujillo D, Morales LA, Chávez D, Trujillo M, Pozo-Espín DF (2025) Enhancing Trajectory Tracking in Humanoid Robots Using Neural Network-Based Dynamic Gain Control
7. Naidu IES, Padmavathi T, Padmavathi SV, Kumar BU (2025) Intelligence based controlling models for effective power tracking and voltage enhancement in grid-pv systems
8. Jia L (2025) Wang, C (2025) Stability of a non-autonomous reaction-diffusion food chain system with feedback control and time-varying delays. Adv Continu Discrete Model 1:115
9. Kharrat M (2024) Neural network-based adaptive fault-tolerant control for nonlinear systems with unknown backlash-like hysteresis and unmodeled dynamics. Communications in Nonlinear Science and Numerical Simulation, pp 108478
10. Lv W (2017) Wang F (2017) Adaptive tracking control for a class of uncertain nonlinear systems with infinite number of actuator failures using neural networks. Adv Diff Equ 1:374
11. Wang Q, Cao J, Liu H (2022) Adaptive fuzzy control of nonlinear systems with predefined time and accuracy. IEEE Trans Fuzzy Syst 30(12):5152–5165
12. Hou T, Zhou J (2024) Observer design and state-feedback stabilization for nonlinear systems via equilibrium manifold expansion linearization. Qual Theory Dyn Syst 23(Suppl 1):254

13. Fang L, Ding S, Park JH, Ma L (2020) Adaptive fuzzy control for nontriangular stochastic high-order nonlinear systems subject to asymmetric output constraints. IEEE Trans Cybern 52(2):1280–1291
14. Wang H, Liu S, Yang X (2020) Adaptive neural control for non-strict-feedback nonlinear systems with input delay. Inf Sci 514:605–616
15. Zhu Q, Liu Y, Wen G (2020) Adaptive neural network output feedback control for stochastic nonlinear systems with full state constraints. ISA Trans 101:60–68
16. Yuan X, Chen B, Lin C (2021) Prescribed finite-time adaptive neural tracking control for nonlinear state-constrained systems: Barrier function approach. IEEE Trans Neural Netw Learn Syst 33(12):7513–7522
17. Niu B, Wang X, Wang X, Wang X, Li T (2024) Adaptive barrier-Lyapunov-functions based control scheme of nonlinear pure-feedback systems with full state constraints and asymptotic tracking performance. J Syst Sci Complexity 37(3):965–984
18. Ding B, Pan Y, Lu Q (2023) Neural adaptive optimal control for nonlinear multiagent systems with full-state constraints and immeasurable states. Neurocomputing 544:126259
19. Jiang Y, Gao W, Chen C, Chai T, Lewis FL (2023) Adaptive optimal control of linear discrete-time networked control systems with two-channel stochastic dropouts. SIAM J Control Optim 61(5):3183–3208
20. Li Y, Liu Y, Tong S (2021) Observer-based neuro-adaptive optimized control of strict-feedback nonlinear systems with state constraints. IEEE Trans Neural Netw Learn Syst 33(7):3131–3145
21. Xin C, Li YX, Ahn CK (2022) Adaptive neural asymptotic tracking of uncertain non-strict feedback systems with full-state constraints via command filtered technique. IEEE Trans Neural Netw Learn Syst 34(10):8102–8107
22. Song S, Jiang Y, Song X, Stojanovic V (2025) Composite neural learning-based adaptive actuator failure compensation control for full-state constrained autonomous surface vehicle. Neural Comput Appl 37(8):6369–6381
23. He K, Dong C, Wang Q (2022) Active disturbance rejection adaptive control for uncertain nonlinear systems with unknown time?varying dead?zone input. Asian Journal of Control 24(3):1209–1222
24. Zong G, Wang Y, Karimi HR, Shi K (2022) Observer-based adaptive neural tracking control for a class of nonlinear systems with prescribed performance and input dead-zone constraints. Neural Netw 147:126–135
25. Song Z, Li P, Wang Z, Huang X, Liu W (2020) Adaptive tracking control for switched uncertain nonlinear systems with input saturation and unmodeled dynamics. IEEE Trans Circ Syst II Expr Briefs 67(12):3152–3156
26. Lei M, Chen W, Wang L (2023) Adaptive tracking control for a class of nonlinear systems with input dead?zone and actuator failure. Mat Methods App Sci 46(6):7333–7352
27. Ma L, Huo X, Zhao X, Zong GD (2020) Observer-based adaptive neural tracking control for output-constrained switched MIMO nonstrict-feedback nonlinear systems with unknown dead zone. Non Dyn 99(2):1019–1036
28. Song Z, Gao L, Wang Z, Li P (2023) Adaptive neural control of constrained MIMO nonlinear systems with asymmetric input saturation and dead zone. IEEE Transactions on Neural Networks and Learning Systems
29. Xu W, Liu X, Wang H, Zhou Y (2022) Event-based adaptive NN controller design for strict-feedback discrete-time nonlinear systems with input dead zone and saturation. Int J Control 95(1):218–233
30. Zong G, Xu Q, Zhao X, Su SF, Song L (2022) Output-feedback adaptive neural network control for uncertain nonsmooth nonlinear systems with input deadzone and saturation. IEEE Trans Cybern 53(9):5957–5969
31. Liu C, Wang H, Liu X, Zhou Y (2020) Adaptive fuzzy funnel control for nonlinear systems with input deadzone and saturation. Int J Syst Sci 51(9):1542–1555
32. Kharrat M, Alhazmi H (2024) Adaptive finite-time neural control of nonstrict-feedback nonlinear systems with input dead-zone and output hysteresis. Int J Gen Syst pp 1–24
33. Fan X, Li Y, Tong S (2024) Finite-time fuzzy adaptive output feedback resilient control of nonlinear cyber-physical systems with sensor attacks and actuator faults. J Syst Sci Compl 37(4):1545–1560
34. Sheng N, Liu Y, Chi R, Ai Z (2024) Adaptive observer-based finite-time fault tolerant control for non-strict feedback systems. JSyst Sci Complex 37(4):1526–1544
35. Tan, L, Wang, X (2024) Finite-Time Neuro-adaptive Controller Algorithms for Nonlinear Multiagent Systems with State Constraints and Unmodeled Dynamics. Cogn Comput, pp 1–11
36. Wang H, Xu K, Zhang H (2022) Adaptive finite-time tracking control of nonlinear systems with dynamics uncertainties. IEEE Trans Autom Control 68(9):5737–5744
37. Shao L, Sun W, Ding L (2024) Finite-time adaptive control of output constrained nonlinear systems under deception attacks. Nonlinear Dyn pp 1–18
38. Mei Y, Wang J, Park JH, Shi K, Shen H (2022) Adaptive fixed-time control for nonlinear systems against time-varying actuator faults. Non Dyn 107(4):3629–3640
39. Yuan X, Chen B, Lin C (2021) Neural adaptive fixed-time control for nonlinear systems with full-state constraints. IEEE Trans Cybern 53(5):3048–3059
40. Chen M, Li Y, Wang H, Peng K, Wu L (2022) Adaptive fixed-time tracking control for nonlinear systems based on finite-time command-filtered backstepping. IEEE Trans Fuzzy Syst 31(5):1604–1613
41. Yang H, Ye D (2020) Adaptive fuzzy nonsingular fixed-time control for nonstrict-feedback constrained nonlinear multiagent systems with input saturation. IEEE Trans Fuzzy Syst 29(10):3142–3153
42. Song J, Chen Y, Liu Y, Zhang L (2023) Fixed-time fuzzy adaptive fault-tolerant control for strict-feedback nonlinear systems with input delay. Syst, IEEE Trans Syst Man Cybern
43. Shen G, Huang P, Ma Z, Zhang F, Xia Y (2023) Dynamic event-based adaptive fixed-time control for uncertain strict-feedback nonlinear systems with state constraints. IEEE Transactions on Cybernetics
44. Wang J, Wang C, Liu Z, Chen CP, Zhang C (2023) Practical fixed-time adaptive ERBFNNs event-triggered control for uncertain nonlinear systems with dead-zone constraint. IEEE Trans Syst Man Cyber Syst 54(1):342–351
45. Wang Z, Wang H, Wang X, Pang N, Shi Q (2024) Event-triggered adaptive neural control for full state-constrained nonlinear systems with unknown disturbances. Cogn Comput 16(2):717–726
46. Wu X, Ding S, Niu B, Xu N, Zhao X (2024) Predefined-time event-triggered adaptive tracking control for strict-feedback nonlinear systems with full-state constraints. Int J Gen Syst 53(3):352–380
47. Li Q, Shen B, Liang J, Shu H (2015) Event-triggered synchronization control for complex networks with uncertain inner coupling. Int J Gen Syst 44(2):212–225

48. Xin C, Li Y, Niu B (2022) Event-triggered adaptive fuzzy finite time control of fractional-order non-strict feedback nonlinear systems. J Syst Sci Complex 35(6):2166–2180
49. Jin X, Li YX (2021) Fuzzy adaptive event-triggered control for a class of nonlinear systems with time-varying full state constraints. Inf Sci 563:111–129
50. Qiu J, Karimi HR, Fu Y (2020) Event-triggered robust fuzzy adaptive finite-time control of nonlinear systems with prescribed performance. IEEE Trans Fuzzy Syst 29(6):1460–1471
51. Wang H, Xu K, Qiu J (2021) Event-triggered adaptive fuzzy fixed-time tracking control for a class of nonstrict-feedback nonlinear systems. IEEE Trans Circ Syst I Regular Papers 68(7):3058–3068
52. Wang C, Wang J, Du Y, Zhang C, Liu Z, Chen CP (2023) Fixed-time event-triggered fuzzy adaptive control for uncertain nonlinear systems with full-state constraints. Inf Sci 633:158–169
53. Bai Z, Li S, Liu H (2023) Composite observer?based adaptive event?triggered backstepping control for fractional?order nonlinear systems with input constraints. Math Methods Appl Sci 46(16):16415–16433
54. Gao L, Song Z, Wang Z (2023) Command-filter-based finite-time event-triggered adaptive output feedback control for nonlinear systems with state-function constraints. J Franklin Inst 360(18):14190–14207
55. You Z, Wang F, Lu X (2023) Event-trigger-based finite-time adaptive fuzzy control for stochastic nonlinear systems with unmeasured states. IEEE Trans Fuzzy Syst 31(12):4529–4541
56. Jiang Y, Liu Z, Chen Z (2023) Fuzzy adaptive finite-time tracking control for a class of nonlinear systems: An event-triggered quantized control scheme. IEEE Trans Fuzzy Syst 31(11):4137–4144
57. Chen Q, Wu LB, Chen M, Liu MR (2024) Fixed?time adaptive event?triggered fault?tolerant control of nonlinear systems with actuator failures. Asian Journal of Control
58. Song X, Sun P, Song S, Stojanovic V (2024) Saturated-threshold event-triggered adaptive global prescribed performance control for nonlinear Markov jumping systems and application to a chemical reactor model. Expert Syst Appl 249:123490